

# When LLMs step into the 3D World: A Survey and Meta-Analysis of 3D Tasks via Multi-modal Large Language Models

Xianzheng Ma \*, Yash Bhalgat \*, Brandon Smart \*, Shuai Chen, Xinghui Li, Jian Ding, Jindong Gu, Dave Zhenyu Chen, Songyou Peng, Jia-Wang Bian, Philip H Torr, Marc Pollefeys, Matthias Nießner, Ian D Reid, Angel X. Chang, Iro Laina, Victor Adrian Prisacariu

**Abstract**—As large language models (LLMs) evolve, their integration with 3D spatial data (3D-LLMs) has seen rapid progress, offering unprecedented capabilities for understanding and interacting with physical spaces. This survey provides a comprehensive overview of the methodologies enabling LLMs to process, understand, and generate 3D data. Highlighting the unique advantages of LLMs, such as in-context learning, step-by-step reasoning, open-vocabulary capabilities, and extensive world knowledge, we underscore their potential to significantly advance spatial comprehension and interaction within embodied Artificial Intelligence (AI) systems. Our investigation spans various 3D data representations, from point clouds to Neural Radiance Fields (NeRFs). It examines their integration with LLMs for tasks such as 3D scene understanding, captioning, question-answering, and dialogue, as well as LLM-based agents for spatial reasoning, planning, and navigation. The paper also includes a brief review of other methods that integrate 3D and language. The meta-analysis presented in this paper reveals significant progress yet underscores the necessity for novel approaches to harness the full potential of 3D-LLMs. Hence, with this paper, we aim to chart a course for future research that explores and expands the capabilities of 3D-LLMs in understanding and interacting with the complex 3D world. To support this survey, we have established a project page where papers related to our topic are organized and listed: <https://github.com/ActiveVisionLab/Awesome-LLM-3D>.

**Index Terms**—3D Scene Understanding, Large Language Models, Vision Language Models, Computer Vision.



## 1 INTRODUCTION

THE advent of Large Language Models (LLMs) has marked a transformative era in natural language processing, enabling machines to understand, generate, and interact with human language in previously unimagined ways. However, the physical world around us is inherently three-dimensional, and understanding spatial 3D environments is crucial for many real-world applications that involve perception, navigation, and interaction within these 3D spaces. With recent advancements, the application of LLMs has extended well beyond text. The fusion of LLMs with 3D data presents a unique opportunity to enhance computational models’ understanding of and interaction with the physical world, leading to innovations across various domains, including autonomous systems [1, 2, 3, 4, 5], augmented reality [6, 7, 8, 9], robotic navigation [10, 11, 12], and robotic manipulation [13, 14, 15].

Recent works have demonstrated the potential of integrating LLMs with 3D data to interpret, reason, or plan in complex 3D environments, by leveraging the inherent strengths of LLMs, includ-

ing zero-shot learning [16, 17], advanced reasoning [13, 18, 19], and extensive knowledge [20, 21]. However, the integration of LLMs with 3D data is not trivial. Issues such as 3D data representation, model scalability, and computational efficiency remain significant hurdles. Moreover, ensuring the models can operate in real-world settings requires overcoming obstacles related to data diversity and environmental complexity. Addressing these challenges is crucial for the full realization of LLMs’ potential in 3D applications to create dynamic and context-aware AI systems.

This survey paper provides a critical examination of the intersection of LLMs with 3D data, offering an exhaustive overview of current methodologies, applications, and challenges in this domain. We start by providing the relevant background on common 3D representations, a brief introduction to LLMs and an overview of Vision-Language Models (VLMs) and Vision Foundation Models (VFMs) in Sec. 2. In Sec. 3, we detail the 3D vision language tasks that current methods aim to solve, outlining the current evaluation metrics and protocols.

Next, in Sec. 4, we analyze the data formats, processing techniques, and model architectures that have shown promise in enhancing 3D understanding through the lens of LLM capabilities. We showcase a variety of areas where the amalgamation of LLMs and 3D data has been successfully demonstrated, such as: using LLMs’ world-knowledge [20, 22] and reasoning capabilities [21, 23] to enhance 3D task performance, using LLMs as multi-modal interfaces [24, 18] and embodied agents [15, 13], or generating complex scenes with LLMs [25, 26]. Beyond LLMs, a few research works have proposed end-to-end architectures that unify 3D perception with language capabilities [27, 28]. Moreover,

\* *Equal contribution. Listing order is random.*

- Xianzheng Ma, Yash Bhalgat, Brandon Smart, Shuai Chen, Xinghui Li, Jindong Gu, Philip Torr, Iro Laina and Victor Adrian Prisacariu are with the University of Oxford.
- Jian Ding is with the King Abdullah University of Science and Technology.
- Dave Zhenyu Chen and Matthias Nießner are with the Technical University of Munich.
- Jia-Wang Bian and Ian D Reid are with the Mohamed bin Zayed University of Artificial Intelligence.
- Angel X. Chang is with Simon Fraser University.
- Songyou Peng and Marc Pollefeys are with ETH Zurich.
- Correspondence e-mail: xianzheng@robots.ox.ac.uk or yashsb@robots.ox.ac.uk

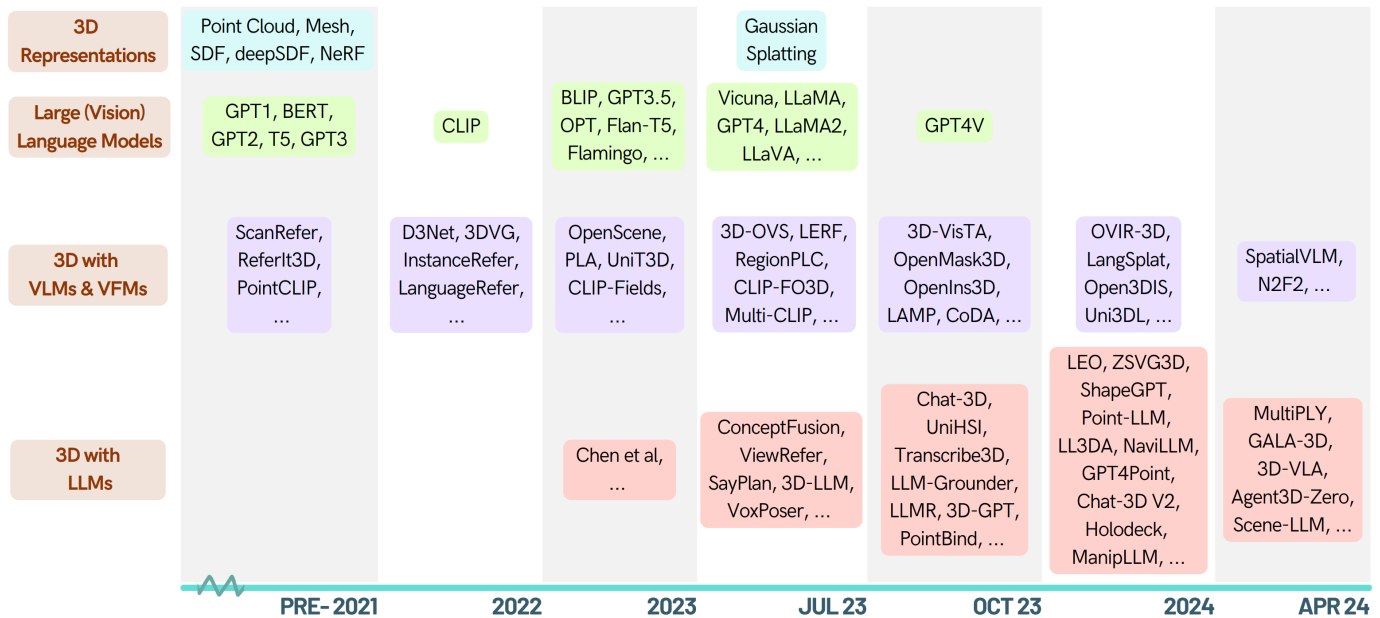


Fig. 1: A general timeline of methods leading up to Large Language Models (LLMs) in 3D.

a wide range of works have explored distilling the knowledge of off-the-shelf 2D Vision Language Models (VLMs) for open vocabulary 3D scene understanding [29, 30] as well as text-driven 3D generation [31, 32]. This survey provides a complete overview of these methods in Sec. 5 to show a complete picture of the field of 3D+Language. We then outline the datasets used to train and evaluate these methods in Sec. 6. Finally, Sec. 7 highlights the challenges and potential future research directions in this field.

## 2 BACKGROUND

This section offers essential background knowledge on 3D representations, Large Language Models (LLMs), 2D Vision-Language Models (VLMs), and Vision Foundation Models (VFMs).

### 2.1 3D Representations

Choosing a 3D representation to describe, model, and understand our world is a crucial topic that contributes to the understanding of the current progress in 3D-LLMs. It is also a fundamental research area in computer vision. The field has recently seen substantial growth due to advancements in deep learning, computational resources, and 3D data availability. We briefly describe the most common 3D representations currently in use.

**Point Clouds** represent 3D shapes with a set of data points in space, storing each point position in a 3D Cartesian coordinate system. In addition to storing the position, other information (*e.g.* color, normal) can also be stored with each point. Point cloud-based methods [33, 34, 35, 36, 37, 38, 39, 40, 41, 42, 43] are noted for their low storage footprint but lack surface topology information. Typical sources for obtaining point clouds include LiDAR sensors, structured light scanners, time-of-flight cameras, stereo-views, photogrammetry, etc.

**Voxel Grids** [44, 45, 46, 47, 48, 49, 50, 51] consist of unit cubes in 3D space, akin to pixel representations in 2D [52]. Each voxel minimally encodes the occupancy information (binary or probabilistically) but can additionally encode distance to a surface, as in the Signed Distance Function (SDF) [53, 54, 55, 56, 57] or

Truncated Signed Distance Function (TSDF) [58, 59, 60, 61, 62, 63]. Nevertheless, the memory footprint can become excessive when high-resolution details are required.

**Polygonal Mesh** representations are composed of vertices and surfaces and describe complex 3D shapes compactly. However, their unstructured and non-differentiable nature [64] poses challenges in integrating them with neural networks for end-to-end differentiable pipelines. Some solutions addressing this problem, such as gradient approximation-based approaches [65, 66, 67, 68], can only use handcrafted gradient calculation. Other solutions like differentiable rasterizers [69, 70, 71] may lead to imprecise render results such as blurry content.

**Neural Fields** [72] have gained a growing interest in the 3D research community over recent years, departing from traditional representations reliant on geometric primitives [73]. A neural field is a mapping from spatial coordinates to scene properties (such as occupancy, color, radiance, etc), but unlike a voxel grid – in which the mapping is from a discrete cell to the value at that voxel – in a neural field the mapping is a learned function, typically a multi-layer perceptron. In this way neural fields implicitly learn compact, continuous, and differentiable 3D shape and scene representations.

One set of neural fields has focused on implicit surface representations. *Occupancy Networks* [74, 75, 76] encode shapes in a continuous 3D occupancy function represented by neural networks, using 3D point locations and features from point clouds, low-resolution voxels, or images to estimate occupancy probabilities. Concurrently, *Deep SDF* networks [77, 78, 79, 80] use neural networks to estimate SDFs from 3D coordinates and latent vectors. Recent methods like *NeuS* [79] and *NeuS2* [80] notably improve surface reconstruction fidelity and efficiency for both static and dynamic objects.

Another set of approaches, referred to as *Neural Radiance Fields* (NeRF) [81, 82, 83, 84, 85, 86, 87, 88, 89, 90, 91, 92, 93, 94], display strong photorealistic rendering capabilities of the 3D world. These methods encode scene details with positional encoding techniques [95, 96, 90, 97], and utilize MLPs to predict

radiance values (color and opacity) along camera rays. However, the necessity for MLPs to infer color and occupancy details for each sampled point in space (including those in empty spaces) requires significant computational resources. Thus, there is a strong incentive to reduce NeRFs’ computational overhead for real-time applications.

**Hybrid Representations** attempt to combine NeRF techniques with traditional volumetric-based approaches, facilitating high quality, real-time rendering [98, 99, 100, 101, 102, 103, 104, 105, 106, 107]. For instance, combining voxel grids [95, 96, 98, 97] or multi-resolution hash grids [102] with neural networks greatly reduces the NeRF’s training and inference time.

**3D Gaussian Splatting** [103, 106, 107] is a variation on point clouds where each point contains additional information representing the radiance being emitted in the spatial region around that point as an anisotropic 3D Gaussian ‘blob’. These 3D Gaussians are typically initialized from SfM point clouds [108], and optimized using differentiable rendering. 3D Gaussian Splatting achieves state-of-the-art novel-view synthesis at a fraction of NeRF’s computation by utilizing efficient rasterization [109] rather than raytracing.

## 2.2 Large Language Model (LLM)

Traditional natural language processing (NLP) encompasses a wide range of tasks aimed at enabling systems to understand, generate and manipulate text. Early approaches in NLP relied on techniques like rule-based systems, statistical models, and earlier neural architectures like recurrent neural networks [110, 111]. The recent introduction of Large Language Models (LLMs), employing transformer architectures [95] and training on vast text corpora [112], has achieved unprecedented performance and sparked a new wave of excitement in the field. Since this paper focuses on 3D LLMs, we provide relevant background knowledge of LLMs here. For an in-depth exploration of LLMs at large, we refer to the latest surveys in the area [113, 114, 115, 116, 117].

### 2.2.1 LLM Architectures

In the context of LLMs, the “encoder-decoder” and “decoder-only” architectures are prominently used for NLP tasks.

**Encoder-decoder architectures** [95, 118, 119] consist of two main components: an encoder  $f_{enc}$  and a decoder  $f_{dec}$ . The encoder and decoder components are typically implemented using transformers [95], which employ attention mechanisms to capture long-range dependencies in the input and output sequences. The encoder takes the input sequence  $X = (x_1, x_2, \dots, x_N)$  and maps it into a sequence of latent representations  $H = (h_1, h_2, \dots, h_N)$  that capture the contextual information, and the decoder generates the output sequence  $Y = (y_1, y_2, \dots, y_T)$  based on  $H$ . Mathematically, the encoding process can be expressed as  $H = f_{enc}(X)$ , and the entire latent sequence  $H$  is generated at once from  $X$ . The decoder, however, generates the output sequence  $Y$  sequentially:  $y_t = f_{dec}(y_{<t}, H)$  where  $y_{<t} = (y_1, y_2, \dots, y_{t-1})$ .

**Decoder-only architectures** [120, 121, 122], on the other hand, are a variant of the transformer architecture that uses only the decoder component. It is particularly suitable for language modeling tasks, where the goal is to predict the next token given the previous tokens. The decoder-only architecture can be mathematically expressed as  $y_t = f_{dec}(y_{<t})$ .

**Tokenization** is a preprocessing method to break the input text into a sequence of tokens, the basic data unit in language models. The number of tokens is finite, and each token can correspond to a word, sub-word, or a single letter. During inference, the input text is converted to a sequence of tokens and fed to the models, which predict the output tokens that are then converted back to text. The tokenization has a great impact on the performance of the language models, as it affects how the models perceive text. Various tokenization techniques are used, such as word-level tokenization, subword tokenization (*e.g.* byte-pair encoding [123], WordPiece [124], SentencePiece [125]), and character-level tokenization [126].

### 2.2.2 LLM Emergent Abilities

One major difference between LLM and traditional non-LLM methods is the emergent abilities that become available in large models but are not present in the small models [115]. The term “*emergent abilities*” refers to new, complex capabilities that arise as LLMs scale in size and complexity. These abilities enable advanced understanding and generation of natural language, problem-solving across various domains without specific training, and adapting to new tasks through in-context learning. In the following, we introduce several common emergent abilities in the scope of LLMs.

**In-Context Learning** [127, 128, 129] refers to the ability of LLMs to understand and respond to new tasks or queries based on the context provided within the prompt, without requiring explicit retraining or fine-tuning. Milestone papers (GPT-2/GPT-3 [130, 127]) demonstrate in-context learning in a few-shot manner, where a model is provided with a few examples of a task within the prompt and then asked to tackle a different example without prior explicit training. State-of-the-art LLMs, such as GPT-4 [131], exhibit remarkable in-context learning abilities, understanding complex instructions, and performing a wide range of tasks from simple translations to generating code and creative writing, all based on the context provided within the prompt.

**Reasoning** in the context of LLMs, often referred to as “chain-of-thought” prompting [132, 133], involves the model generating intermediate steps or reasoning paths when tackling complex problems or questions. This approach allows LLMs to break tasks into smaller, manageable parts, facilitating a more structured and understandable solution process. To achieve this, training involves datasets that include a variety of problem-solving tasks [134, 135], logical puzzles [136, 137], and datasets designed to mimic reasoning under uncertainty [138]. Current state-of-the-art LLMs [127, 131, 139, 140, 141, 142, 143] demonstrate advanced reasoning capabilities typically when model sizes become larger than 60B to 100B parameters [132].

**Instruction-following** [144, 127, 140, 145, 146] refers to the models’ capability to understand and execute commands, or follow instructions as specified by the user. This involves parsing the instruction, understanding its intent, and generating an appropriate response or action. Methods for adapting this ability to novel tasks may require instruction tuning from datasets [114] containing various instructions paired with correct responses or actions. Techniques such as supervised learning, reinforcement learning from human feedback, and interactive learning can further enhance performance.

### 2.2.3 LLM Fine-tuning

In the context of 3D-LLMs, LLMs are either utilized directly in their pre-trained state or undergo fine-tuning to accommodate novel multi-modal tasks. However, fine-tuning the entirety of an LLM’s parameters presents significant computational and memory challenges due to the large amount of parameters involved. Therefore, parameter-efficient fine-tuning (PEFT) [147] has become increasingly popular for adapting LLMs to specific tasks by updating only a relatively small subset of the model’s parameters instead of retraining the entire model. The following part lists four common PEFT methods used in LLMs.

**Low-Rank Adaptation (LoRA)** and variants [148, 149, 150] update parameters through low-rank matrices. Mathematically, a forward pass for LoRA [148] during the fine-tuning can be expressed as  $h = W_0x + BAx$ .  $W_0$  is the frozen weight of LLM, while  $BA$  is a low-rank matrix parameterized by newly introduced matrices  $A$  and  $B$ , which are updated at fine-tuning stages. This method offers several distinct benefits. During fine-tuning, only  $B$  and  $A$  are optimized, significantly reducing the computational overhead associated with gradient calculation and parameter updates. Once the fine-tuning concludes and the weights are merged, there is no additional inference cost compared to the original model, as represented by the equation:  $h = (W_0 + BA)x$ . Moreover, there’s no need to save multiple copies of LLMs for different tasks since multiple LoRA instances can be saved instead, reducing the storage footprint.

**Layer Freezing** [151, 142, 152] freezes selected layers of a pre-trained model while updating others during training. This often applies to layers closer to the model’s input or output, depending on the task’s nature and the model architecture. In 3D-LLM methods, for example, all layers except input and output embeddings [153] might be frozen to mitigate overfitting risks with task-specific datasets, retaining the pre-trained general knowledge and reducing parameters that need to be optimized.

**Prompt Tuning** [154, 155, 156] guides LLMs to perform specific tasks by framing them within prompts, adjusting model inputs in contrast to conventional fine-tuning which adjusts model parameters. Manual prompt engineering [132, 157, 158, 159] is the most intuitive method, yet it is difficult for experienced prompt-tuning engineers to find the optimal prompt. Another set of approaches is automatic prompt generation and optimization. One prevalent approach is to search for the exact optimal input prompt text, known as *hard prompt*, such as [160, 161, 162, 163]. Alternatively, one can use optimization approaches to optimize the embedding of the prompt (*soft prompt*) [154, 164, 165, 166, 167, 168, 169, 170].

**Adaptive Fine-tuning** customizes the model architecture for specific tasks by adding or removing layers or modules [171, 172, 173]. This can include integrating new data modalities, such as visual information, alongside textual data. The core idea of adaptive fine-tuning is leveraging small neural network modules inserted between the layers of a pre-trained model. During adaptive fine-tuning, only the parameters of these adapter modules are updated, while the original model weights remain fixed.

## 2.3 2D Vision-Language models

Vision-Language Models are a family of models which aim to capture and exploit the relationship between text and images/video, and are capable of performing interactive tasks between the two modalities. The majority of VLMs have

transformer-based architectures. By leveraging the attention module, visual and textual contents are conditioned on each other, which enables mutual interaction. In the following paragraphs, we briefly cover the applications of VLMs to discriminative and generative tasks.

**Discriminative tasks** involve predicting a certain characteristic about the data. VLMs, such as CLIP [174] and ALIGN [175], have shown exceptional performance in zero-shot transferability to unseen data in image classification. Both models comprise two modules: a visual encoder and a text encoder. Given an image and its category, CLIP and ALIGN are trained by maximizing the similarity between the image embedding and the textual embedding of the sentence “a photo of a  $\{image\ category\}$ ”. The zero-shot transferability is achieved by replacing “ $\{image\ category\}$ ” with possible candidates during inference and searching for sentences matching best with the image. These two works have inspired numerous follow-ups such as [176, 177, 178, 179], which further boost image classification accuracy. The models can also distill learned knowledge for other tasks, including object detection [180, 181, 182, 183], image segmentation [184, 185, 186, 187, 188], document understanding [189, 190] and video recognition [191].

**Generative tasks** utilize VLMs to generate text or images from input data. By leveraging large-scale training data, a single VLM can usually perform several image-to-text generation tasks, such as image captioning and visual question answering (VQA). Notable examples include SimVLM [192], BLIP [193], and OFA [194], *etc.* More powerful VLMs such as BLIP-2 [195], Flamingo [196], and LLaVA [197], are able to handle multi-turn conversations and reasoning based on the input image. Following the introduction of the diffusion model, text-to-image generation has also become a focus of the research community [198, 199]. By training on a large amount of image-text pairs, diffusion models [200, 201] can generate high-quality images based on textual input. This capability has also been extended to generating videos [202], 3D scenes [31], and dynamic 3D objects [203]. Along with generative tasks, it is also possible to edit existing images through the textual prompt [204, 205, 206, 207].

## 2.4 Vision Foundation Models (VFMs)

Vision Foundation Models (VFMs) are large neural networks that aim to extract image representations that are sufficiently diverse and expressive to be directly deployed in various downstream tasks, mirroring the role pre-trained LLMs serve in downstream NLP tasks. One notable example is DINO [208], which uses a self-supervised teacher-student training paradigm. The representation learned achieves good results on both image classification and semantic image matching. The attention weights in DINO can also serve as segmentation masks for semantic components of the observed scene. Followup works like iBOT [209] and DINOv2 [210] further improve the representation by introducing the masked image modeling (MIM) loss. SAM, a transformer-based image segmentation model [211], is trained on a dataset consisting of 1.1 billion images with semantic masks and demonstrates strong zero-shot transfer capability. DINO (Zhang et al.) [212] – not to be confused with DINO (Caron et al.) [208] – employs a DETR-like [213] architecture and mixed query selection for object detection. The follow-up work Grounding-DINO [214] introduces text supervision to boost accuracy. Stable Diffusion [201], a text-to-image generator, has also been used as a feature extractor for ‘real’

images by running a single diffusion step on clean, or artificially noised images and extracting intermediate features [215, 169] or attention masks [216]. These features have been recently used for segmentation [216] and image matching [215, 169] tasks, due to the size and diversity of the training sets used for diffusion models, and due to observed emergent properties of diffusion features, such as zero-shot correspondence across images [215].

### 3 TASKS AND METRICS

To understand the role of language in 3D understanding, it is important to first understand the tasks that 3D vision-language models attempt to solve. Research has grown to include a broad spectrum of research tasks, each with their own set of commonly used datasets and evaluation metrics. Here, we aim to list current 3D vision-language tasks, and their corresponding evaluation metrics. We broadly categorize the tasks by their input and output modalities.

We then begin our analysis of methods for solving these tasks in Sec. 4 and Sec. 5. Then, in Sec. 6, we detail the datasets that are currently used for training and evaluation for these tasks.

#### 3.1 3D Captioning (3D $\rightarrow$ Text)

Given the 3D data of a scene or object, the task of 3D captioning is to generate a corresponding short, natural language description. Here, we decompose this task into a few common variants of the problem, based on the type of data being captioned, and the type of captions that are generated.

**Object-Level Captioning** requires the model to generate a short, natural language description of a single 3D object. This caption should focus on the key characteristics of the object, including its shape and semantic characteristics.

**Scene-Level Captioning** refers to the task of generating a short, natural language caption for an entire 3D scene. These captions typically focus on global scene information (such as room types and styles), key objects in the scene, and their relationships. We consider “grounded captioning”, where the model outputs a description of the relationships between objects in the scene, potentially alongside positional information for those objects, to be a variant of scene captioning.

**3D Dense Captioning** refers to the joint task of localizing instances of objects in a 3D scene and describing them using natural language captions. In this instance, the output may also contain positional information about the objects being captioned. Often, the referring descriptions from 3D grounding datasets are used to produce the captioning and location data needed for 3D dense captioning. For example, captions in Scan2Cap [217] are generated using the referring expressions from ScanRefer [218].

**Evaluation Metrics** for 3D captioning require comparing the generated captions against ground truth captions for testing samples.

Exact Match (EM) requires that the generated caption exactly matches the ground truth. Exact Match has different accuracy thresholds, denoted as  $EM@K$ , which means that the correct answer is within the top “ $K$ ” answers generated by the model. Commonly used thresholds are  $EM@1$  and  $EM@10$ . However, natural language captions with the same semantic meaning can be represented in many ways, so the dominant metrics for captioning are automated text generation metrics [219] that aim to measure matching n-grams or semantic similarity rather than complete sentence matches. BLEU [220] matches n-grams between the predicted and true captions, with “BLEU@ $x$ ” referring to matching

n-grams of length “ $x$ ” (typical values are in the range 1-4). This still requires matching exact words, but is slightly more robust to rearrangements in phrasing. ROUGE [221] similarly aims to match n-grams, with the commonly used ROUGE-L focusing on the structural similarity of sentences. METEOR [222], is based upon the precision and recall of unigram matches, with “matches” also existing between synonyms and words which are morphological variants of each other. CIDEr [223] weights n-grams by their frequency, with higher frequency n-grams given lower weights. As the above metrics rely on n-gram matches, they cannot account for different by semantically similar words. Thus, various metrics that measures semantic content overlap via similarity in learned embedding spaces (*e.g.*, SentenceSim [224] and BERT Score [225]) have been introduced.

For dense captioning, where captions are localized to parts of the scene, adjusted benchmarks are needed. Often, BLEU, ROUGE, METEOR and CIDEr scores are still used, however the score is set to zero if the intersection over union (IoU) between the predicted bounding box and the object is less than a threshold “ $k$ ”. Typical “ $k$ ” values are 0.25 and 0.5 [19, 217, 226]. However, these metrics focus on the captioning recall while ignoring false positives. This is addressed by more recent work that additionally measures the precision and F-1 score of generated captions w.r.t. the BLEU, ROUGE, METEOR and CIDEr metrics [227].

#### 3.2 3D Grounding (3D + Text $\rightarrow$ 3D Position)

Given a 3D scene and a “referring expression” that describes an object in the scene relative to other objects, 3D grounding involves generating a position, bounding box or segmentation mask for the target object(s).

**Single-Object Grounding** involves locating a single query object in a scene given reference information, such as language descriptions [218, 228] or additional gestures [229].

**Multi-Object Grounding** involves locating multiple objects using a referring expression. There are two main variants for this kind of grounding. The first involves a single-sentence description that may be ambiguous, potentially referring to zero, one, or multiple target objects of the same category in the 3D scene [230]. The second variant uses paragraph-length referring expressions that describe multiple objects belonging to potentially different categories, and the spatial relationships between them [231].

**Evaluation Metrics** for 3D grounding require comparing predicted locations, most often in the form of bounding boxes, with ground truth locations of objects from testing samples.  $Acc@KIoU$  [218] is the widely used metric in 3D visual grounding, which measures the percentage of positive predictions which have a intersection over union (IoU) with the ground truth greater than a threshold  $K$ , which is usually set to 0.25 or 0.5. It is worth noting that some datasets evaluate the performance in different scenarios. For example, ScanRefer [218] divides the datasets into unique/multiple/overall splits. Some methods measure the average IoU [153, 232] whereas other methods measure the average distance between the centers of the bounding boxes [153]. For multi-object grounding, the F1 score is used as the metric [230]. They first get the one-to-one matching between the predicted and ground truth bounding boxes according to IoUs. Then the pairs with IoUs higher than a threshold are regarded as true positives.

#### 3.3 3D Conversation (3D + Text $\rightarrow$ Text)

It is also natural to consider tasks where questions are asked about a 3D scene, either in a single-turn setting or a more natural multi-

turn conversational setting.

**3D Question Answering (3D-QA)** is a task where the model is required to generate answers to questions asked by users given a 3D scene. The topic of questions has a diverse range and the model has to understand both the 3D scene and the question to generate the correct response. The question includes both simple tasks such as determining the existence of an object and more difficult ones like spatial reasoning. As there are several well-established benchmarks, and the majority of questions in the benchmarks are factual with unique answers, 3D-QA is a popular task to evaluate a multi-task model’s capability.

**3D Situated Question Answering (3D-SQA)** is a special case of 3D-QA. The key difference is that 3D-QA requires the model to answer questions from the perspective of a spectator with access to all information about the scene, while 3D-SQA needs the answer from the perspective of a player in a pre-defined situation. For example, 3D-SQA may ask “how many chairs are in front of me?” given the situation of “standing behind and facing the dining table”.

**3D Dialogue** requires the model to have a coherent and natural multi-turn conversation with users about the 3D scene, instead of one round QA. For example, a user may want to know about a room, so they continuously ask questions about each part of the room, while the model is expected to respond correctly and coherently.

**Evaluation Metrics** involve comparing a model’s responses with ground truth responses for testing samples. For 3D-QA and 3D-SQA, the dominant metric is the Exact Match (EM), meaning that the answer generated by the model must exactly match with the correct answer. This is because the majority of questions in existing 3D-QA benchmarks [233, 234, 235, 236] are factual questions where there is only one definitively correct answer. For 3D Dialogue and Task Planning whose answers are non-unique, the semantic metrics such as BLEU [220], ROUGE [221], METEOR [222], CIDEr [223], and SPICE [237] are applied to evaluate the similarity between generated responses and reference answers provided by benchmarks. They are also used in 3D-QA, particularly the ScanQA benchmark, to measure the semantic similarity alongside the accuracy.

### 3.4 3D Embodied Agents (3D + Text $\rightarrow$ Action)

It is also useful to consider tasks that involve interactions with the 3D scene, conditioned on a specific text prompt describing the desired action or goal.

**3D Task Planning** is the task where users provide a high-level objective and the model is required to outline low-level steps to fulfill this objective. For example, given a 3D scene of a room, users may ask how to clean the room and the model needs to offer detailed steps to clean it.

**3D Navigation** refers to the task of enabling 3D agents, such as robots or virtual characters, to move and orient themselves within 3D spaces. This involves understanding and interpreting the 3D environment, identifying obstacles, and planning safe, efficient paths to reach designated goals.

**3D Manipulation** refers to the ability of 3D agents to physically interact with objects in their environment. This can range from picking up and moving objects to more complex sequences of actions such as assembling parts or opening doors.

**Evaluation Metrics** for 3D Task Planning also rely on matching the textual/token output of a model with the ground truth actions

for test samples. BLEU [220], ROUGE [221], METEOR [222], CIDEr [223], and SPICE [237] are applied to evaluate the similarity between generated responses and ground-truth answers.

For 3D Navigation, there are two primary metrics to evaluate the performance. 1) Success Rate (SR) measures whether the 3D agent reaches the target locations within a predefined distance threshold. 2) Success Rate Weighted by Path Length (SPL) [238], which is calculated as the SR weighted by the ratio of the ground truth length and actual path length, aims to reflect how efficiently the model achieved its goal. Other metrics include Oracle Success Rate (OSR), Trajectory Length (TL) and Goal Process (GP) [239]. In addition to the above metrics that measure whether the agent successfully reached the target and its efficiency, it is also useful to consider how well the agent path matched the path specified by the language (when language is used to specify a detailed paths). One such metric is Success weighted by normalized Dynamic Time Warping (SDTW) [240] which combines the SR with the difference between the agent path and a ground truth path for a given instruction. Please note that our discussion focuses exclusively on metrics used within 3D-LLMs methods. We encourage readers to refer to Gu *et al.* [241] for summary of navigation metrics.

For 3D Manipulation, the key metric is Success Rate [242], which for manipulation is defined as the number of successful manipulations divided by the total number of task samples. As discussed in Sec. 4.5, different datasets have different conventions for how their actions are represented using text, such as using structured outputs, using normalized numeric scores, or introducing new tokens.

### 3.5 Text-to-3D Generation (Text $\rightarrow$ 3D)

Beyond using text to describe and interact with existing 3D scenes, it is also possible to generate 3D objects and scene via language specification. Here we give a brief summary of this area, see Lee *et al.* [243] for a more in-depth survey.

**3D Object Generation** involves generating 3D models of individual objects from text descriptions. The text input can provide details about the object’s category, attributes, part structure, and other properties that should be reflected in the generated 3D shape.

**3D Scene Generation** is the task of creating full 3D environments such as rooms or outdoor spaces based on text scene descriptions. This involves generating 3D models for objects specified in the text as well as intelligently arranging and composing multiple 3D object models given the constraints specified in the text, like object categories, counts, spatial relationships, and scene attributes.

**3D Editing** refers to modifying existing 3D assets like shapes or scenes based on text instructions. This could involve adding, removing, or transforming objects, changing materials or colors, or altering high-level scene properties according to the given text.

**Evaluation Metrics** for 3D generation tasks assess the quality of the generated shape/scenes and how well the generated content matches the input text. Common metrics to measure generated geometry include Chamfer Distance (CD) and Mesh-Volume/Surface Distance (MVD). CD is calculated by summing squared point-to-point distances w.r.t. ground-truth 3D data, while MVD calculates the volume/surface between two meshes to measure the geometric error. To assess overall quality, classification accuracy checks if semantic properties are preserved, while the Fréchet Inception Distance (FID) captures realism and diversity. To check if the generated shape matches the input text, it is common to measure the similarity of the text with either aligned embeddings of the 3D

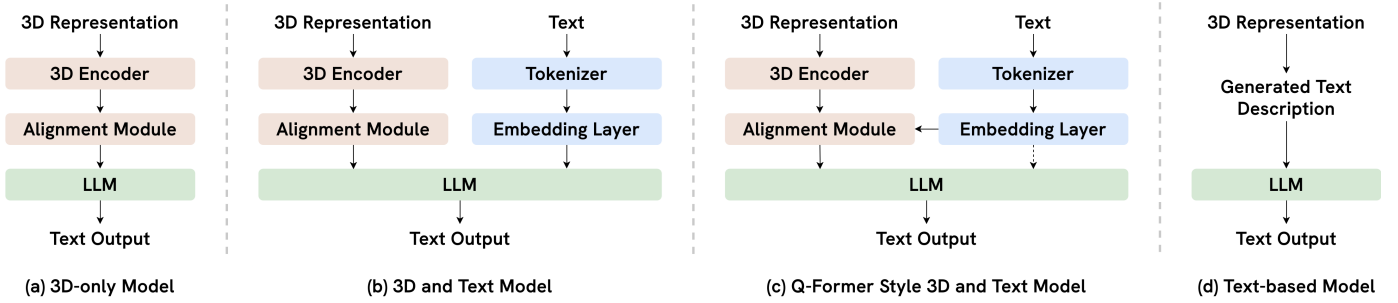


Fig. 2: **Architectures for aligning 3D with text for LLMs.** Here we show four high-level architectures: (a) 3D-only model that aligns 3D features to the LLM’s input space, (b) 3D+text model where 3D features and text are both aligned, (c) Q-Former style model where text is used during to condition the alignment of the 3D features, and optionally given to the LLM itself (dashed arrow), and (d) text-only approach which converts 3D representations into text strings, avoiding the need to train an alignment module.

shape (*e.g.* ULIP [244]) or rendered images (*e.g.* CLIP [174]). It is also common to use human studies for evaluation. However, recent work [245] has shown it is possible to use LVLMs like GPT-v4 as alternative to using human judges. For text-based 3D editing, CD and IoU evaluate how well instructed edits were applied to input geometry without excessive distortion.

## 4 3D TASKS WITH LLMs

3D scene understanding tasks have been widely studied. At its core, scene understanding entails recognizing and categorizing all objects present within a designated 3D environment, a process known as semantic [246, 247, 248, 46, 249, 250] or instance-level [251, 252, 253, 254, 255, 256, 257] understanding. This stage is critical, as it forms the basis upon which more nuanced interpretations are built. Subsequently, a higher level of scene understanding focuses on spatial understanding, which refers to the construction of spatial graphs [258, 259] and the semantics of object relationships [260, 261]. Going further, potential interactions can be predicted, such as affordances [262, 13, 14, 15, 263], scene changes [264, 265], and understanding the broader context of the scene, *e.g.* the functionality and aesthetic styles [266]. 3D data also presents unique challenges that are not present in 2D, such as the relatively high cost of obtaining and labeling 3D data, sparse 3D data structures that are not uniformly dense or aligned to a grid, and the need to reconcile multiple (possibly occluded) viewpoints of the same objects [261, 256]. To this end, researchers have leveraged the power of language, where the semantics and relationships within a 3D world can be embedded. Recent efforts in integrating Large Language Models (LLMs) with 3D data have shown promise in achieving multi-level understanding and interaction, leveraging LLMs’ inherent strengths, namely zero-shot learning, in-context learning, step-by-step reasoning, and extensive world knowledge.

In Sec. 4.1, along with Fig. 2, we provide a brief description of how LLMs process 3D scene information, highlighting how 3D features are aligned with language so that they can be interpreted and reasoned with via LLMs, which is foundational for subsequent sections. The rest of this section is structured to align the taxonomy presented in Fig. 3, which describes the role LLMs have played in solving 3D tasks. We start by showing how the world-knowledge (sometimes referred to as ‘common-sense knowledge’) and reasoning abilities of LLMs can enhance performance on 3D tasks in Sec. 4.2. In Sec. 4.3, we elaborate on how to integrate multiple 3D tasks into one LLM to achieve multi-task learning.

We explore how LLMs can be used as a unified interface for combining other modalities in Sec. 4.4. We then describe how LLMs serve as embodied agents to interact with the 3D world in Sec. 4.5. Finally, we present how LLMs serve as assistants for generating semantically diverse 3D objects and scenes in Sec. 4.6.

In addition, we provide Tab. 1 to contrast 3D-LLMs methods across three axes: 3D components, LLMs components, and the alignment of 3D vision and language, aiming to offer a high-level insight into the various approaches within this evolving field.

### 4.1 How do LLMs process 3D scene information?

Traditional LLMs are limited to text as both input and output, making the ability to ingest 3D information a primary concern for all 3D-LLM methods. The general idea is to map 3D objects or scene information into the language space, enabling LLMs to understand and process these 3D inputs. Specifically, this typically involves two steps: (i) using a pre-trained 3D encoder to process the corresponding 3D representations, yielding original 3D features; (ii) employing an alignment module to translate these 3D features into 3D tokens that LLMs can process, akin to the tokenization process mentioned in Sec. 2.2.1. Pre-trained LLMs can then use these aligned 3D tokens when generating outputs.

Given the diversity of 3D representations, as described in Sec. 2.1, there are multiple ways to obtain 3D features. As shown in 3D Geometry column in Tab. 1, *Point Clouds* [21, 24, 19, 171, 172, 267, 268, 269, 153, 270, 271, 266, 272] are most common due to their simplicity and compatibility with various pre-trained 3D encoders, which makes them a popular choice for multi-task and multi-modal learning methods. *Multi-view Images* [11, 14, 17, 20, 270, 273] are also frequently used as research on 2D feature extraction is well-established, which means that 3D feature extraction requires only an additional 2D to 3D lifting scheme. *RGB-D* data, readily obtained using depth cameras, is commonly used in 3D embodied agent systems to extract viewpoint-relevant information for navigation and understanding. *3D Scene Graphs* are a more abstract 3D representation, excelling in modeling the presence of objects and their relationship, and capturing high-level information of scenes. They are often utilized in 3D scene classification [274] and planning tasks [275]. *NeRFs* are currently less used in 3D-LLM methods [21]. We believe this is due to their implicit nature which makes them more difficult to tokenize and integrate with feed-forward neural networks.

Current methods use different architectures (see Fig. 2) and modules that align 3D features with LLM input spaces (see

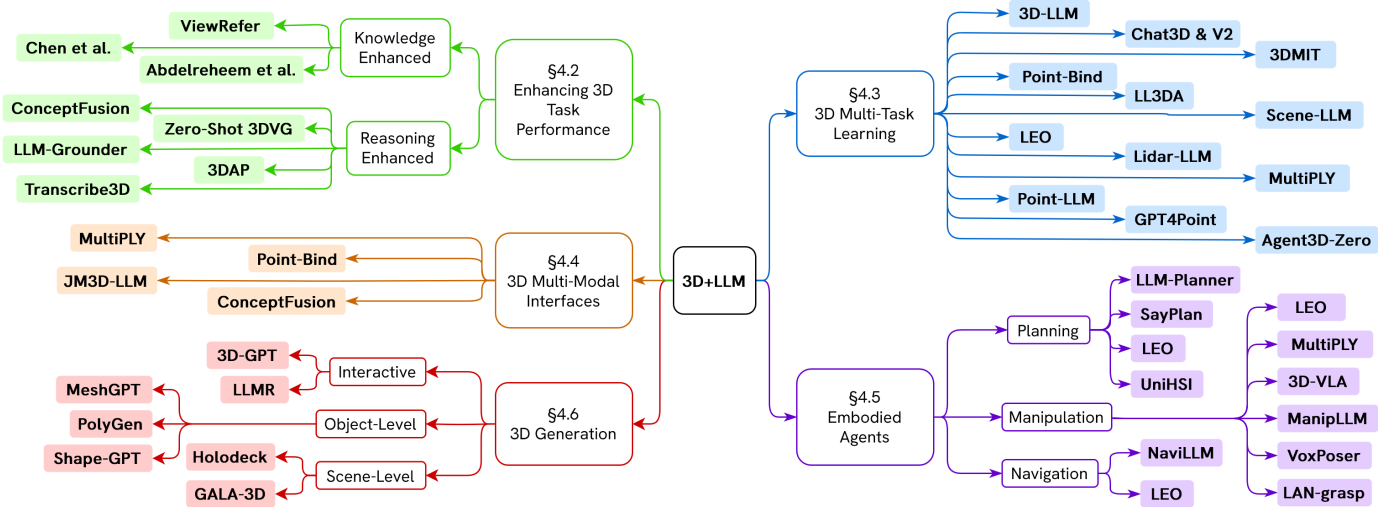


Fig. 3: **Taxonomy of 3D with LLM methods.** In Sec. 4, we analyze the role LLMs have played in solving 3D tasks from five perspectives : **Enhancing 3D Tasks**, **Multi-Task Learning**, **3D Multi-modal Interfaces**, **Embodied Agents**, and **3D Generation**.

3D+LLM column in Tab. 1). For models which only accept 3D inputs (Fig. 2a), a linear layer [269, 24, 266] or an MLP [171, 172] is used as the alignment module to transform 3D features into the LLM input space. Models which accept 3D and text as input often use two separate branches to align 3D features and text (Fig. 2b). Some works [171, 172] employ a one-layer vanilla transformer to allow 3D object features to attend to each other during alignment. Others, such as [270, 271], create transformer-based alignment modules, where the standard transformer architecture is tweaked to better suit the different types of 3D data, such as dense point clouds and sparse LiDAR scans. Meanwhile, text is encoded using the pre-existing LLM text embedding table. Other works [153, 268, 276] follow the Q-Former style approach of [195] to align 3D features and text (Fig. 2c), introducing fixed length query tokens as additional input, and following a BERT-based structure to facilitate interaction between 3D and text features during alignment. Mostly, these three types of architectures described above achieve alignment by utilizing 3D captioning datasets [218], where the captioning loss, *i.e.* the cross-entropy loss between captions generated by LLMs and the brief, ground truth description of the scene, is used to fine-tune the alignment module, while freezing the pre-trained 3D feature extractor and LLM.

Finally, some models [21, 20, 22, 23, 273, 12, 275, 277, 14, 17] employ closed-sourced models like ChatGPT and do not train an alignment module at all (Fig. 2d). Instead of aligning 3D features with the LLM input space, text descriptions are directly generated from the 3D data, such as by describing 3D bounding boxes, positions and relationships, or by using pre-existing captions. These text descriptions are input into ChatGPT. No additional alignment module is proposed in these works, and thus no training is required.

## 4.2 LLMs for Enhancing 3D Task Performance

LLMs trained on large amounts of data have been shown to acquire common-sense knowledge about the world [278]. The potential of LLMs’ world knowledge and reasoning capabilities has been explored to enhance 3D scene understanding and reformulate the pipelines of several 3D tasks. In this section, we focus on methods which aim to use LLMs to improve the

performance of existing methods on 3D vision-language tasks. When applying LLMs to 3D tasks, we can categorize their use into two distinct groups: *knowledge-enhanced* and *reasoning-enhanced* approaches. Knowledge-enhanced approaches tap into the vast world knowledge embedded within LLMs to enhance 3D task performance. This may provide contextual insights, filling in knowledge gaps, or might enhance the semantic understanding of 3D environments. Alternatively, rather than relying on their world knowledge, reasoning-enhanced approaches leverage the ability of LLMs to infer step-by-step, thereby offering better generalization to tackle more complex 3D challenges. The following two sections describe these approaches respectively.

### 4.2.1 Knowledge-enhanced approaches

There are several methods that utilize LLM world knowledge. Chen *et al.* [274] use LLMs for 3D room classification from RGB-D images. Here, the knowledge embedded in LLMs is used to determine the room category based on the object category information contained in the room. Firstly, this approach creates scene graphs from Matterport3D [285] data with nodes for regions and objects, and object nodes linked to room nodes. Next, key objects are selected to form queries per room type. LLMs score descriptions extracted from the selected objects, with the highest score predicting the room label. Spatial information like sizes or locations can also be provided.

ViewRefer [20] uses LLMs to expand the grounding texts with view-related descriptions. For instance, given the original text “Facing the front of the couch, the table that is to the right of the couch”, the LLM is used to create a similar sentence but from another speaker’s point of view, *e.g.* “With back to the front of the couch, pick the table that is on the left side of the couch”. By rephrasing input texts and their opposite-view synonyms several times, the model improves cross-view grounding. It also adopts a fusion transformer with inter-view attention and includes learnable multi-view prototypes, which capture inter-view knowledge and further boost 3D grounding performance.

Abdelreheem *et al.* [22] address the problem of semantic correspondence in 3D shapes. They classify 3D shapes by feeding rendered views into a BLIP2 model to generate lists of class proposals. ChatGPT [286] unifies these into a single class per

Method	Subsection	3D Component			LLM Component				3D+LLM	Date	
		3D Geometry	Vision Model	Tuning	LLM Abilities	Fine-tuning	LLM Base	# Parameters			Hardware
Chen <i>et al.</i> [274]	3.2	SG	CLIP	F	WK	None	GPT2	1.5B	1 RTX3080	-	09/22
ConceptFusion [18]	3.2/3.4	RGB-D	OpenSeg	F	IF/R	None	GPT3	175B	1 3090	-	02/23
ViewRefer [20]	3.2	MVI	Multi-View Transformer	T	WK	None	GPT3	175B	4 A100	Transformer	03/23
LLM-Grounder [21]	3.2	PC/NeRF	OpenScene/LERF	F	IF/ICL/R	None	GPT3.5/4	-	-	-	09/23
Abdelreheem <i>et al.</i> [22]	3.2	Mesh	Vision Transformer	F	IF/WK	None	GPT3.5	-	1 3090	-	09/23
Transcribe3D [23]	3.2	PC	Groupfree Transformer	F	IF/R	None	GPT3.5/4	-	-	-	10/23
zero-shot 3DVG [16]	3.2	RGB-D	Mask3d	F	IF/ICL/R	None	GPT3.5/4	-	-	Transformer	11/23
3DAP [273]	3.2	MVI	-	-	IF/ICL	PT	GPT4V	-	-	-	12/23
3D-LLM [153]	3.3	PC	Mask2Former/SAM	F	IF/ICL/R	LF	OPT/Flan-T5	9B/2.7B/3B	64 V100	QFormer	07/23
Chat-3D [171]	3.3	PC	Point-BERT	F	IF/ICL/R	AF	Vicuna	7B	-	Linear layer	08/23
LEO [270]	3.3	PC/MVI	OpenClip/PointNet++	F	IF/ICL/R	LoRA	Vicuna	7B	8 A100	Transformer	11/23
LL3DA [19]	3.3	PC/3D-BB	ScanNet scene encoder	F	IF/ICL/R	AF	OPT	1.3B	8 3090	QFormer	11/23
Point-LLM [267]	3.3	PC	Point-BERT	F	IF/ICL/R	Full	LLaMA	7B/13B	8 A100	Linear layer	12/23
GPT4Point [268]	3.3	PC	Point-BERT	F	IF/ICL/R	LF	OPT/Flan-T5	6.7B/3B	8 A100	QFormer	12/23
Chat-3D v2 [172]	3.3	PC	Uni-3D	F	IF/ICL/R	AF	Vicuna	7B	4 A40	MLP	12/23
LiDAR-LLM [271]	3.3	PC/VM	VoxelNet	F	IF/ICL/R	AF	LLaMA	7B	4 A100	Transformer	12/23
3DMMIT [269]	3.3	PC	EPCL/Uni3D	F	IF/ICL/R	LoRA	Vicuna	7B	8 A100	Linear layer	01/24
Scene-LLM [266]	3.3	PC/VM	ConceptFusion	F	IF/ICL/R	LF	LLaMA-2	7B	32 A100	Linear layer	03/24
Point-Bind [272]	3.4	PC	I2P-MAE	F	IF/ICL/R	LF	LLaMA	7B	8 A100	Linear layer	09/23
JM3D-LLM [279]	3.4	PC	PointNet++/PointMLP/Point-BERT	F	IF/ICL/R	LF	Vicuna	7B	3 A100	MLP	10/23
LLM-Planner [12]	3.5	VM	Seg&Depth	F	IF/ICL/R	None	GPT3	175B	-	-	03/23
SayPlan [275]	3.5	SG	SG generator	F	IF/ICL/R	None	GPT4	-	-	-	07/23
VoxPoser [13]	3.5	RGB-D	OWL-ViT/SAM	F	IF/ICL/R	None	GPT4	-	-	-	07/23
UniHSI [277]	3.5	RGB-D	-	-	IF/ICL/R	None	GPT3.5/4	-	1 A100	-	09/23
LAN-grasp [14]	3.5	MVI	OWL-ViT	F	IF/ICL/R	None	GPT4	-	-	-	10/23
Agent3D-Zero [17]	3.3/3.5	MVI	-	-	IF/ICL/R	PT	GPT4V	-	-	-	03/24
NaviLLM [11]	3.5	MVI	EVA-CLIP-Large	F	IF/ICL/R	LF	Vicuna	7B	8 A100	Transformer	12/23
MultiPLY [24]	3.3/3.4/3.5	PC	ConceptGraph	T	IF/ICL/R	AF	Vicuna	13B	128 V100	Linear layer	01/24
ManipLLM [15]	3.5	RGB-D	CLIP	F	IF/ICL/R	AF	LLaMA	7B	1 A100	Linear layer	03/24
3D-VLA [276]	3.3/3.5	PC/MVI	Mask2Former/SAM	F	IF/ICL/R	LoRA	Flan-T5	3B	384 V100	QFormer	03/24
PolyGen [280]	3.6	<i>n</i> -gon Mesh	Custom Transformer	F	-	Full	Custom	-	4 V100	-	02/20
LLMR [281]	3.6	Unity, Mesh	Dall-E-2, CLIP	F	IF/ICL/R	None	GPT4	-	1 3080	-	09/23
3D-GPT [26]	3.6	Blender, Mesh	-	-	IF/R	None	GPT3.5/4	-	-	-	10/23
MeshGPT [282]	3.6	Mesh	GPT-2-style Transformer	F	-	Full	GPT-2-style	~345M	4 A100	-	11/23
ShapeGPT [283]	3.6	SDF	3D VQ-VAE, CLIP	F	IF/R	Full	T5	-	4 A100	T5	11/23
Holodeck [284]	3.6	Mesh	-	-	IF/R	None	GPT4	-	8 RTX 8k	CLIP/SBERT	12/23
GALA-3D [25]	3.6	3DGS	MVDream, Control-Net	F	IF/R	None	Any (GPT3.5)	-	-	-	02/24

TABLE 1: **Summarization of 3D-LLMs methods.** The *3D Geometry* column collects the 3D geometric information being used for each method, such as Point Cloud (PC), Multi-view Images (MVI), RGB+Depth (RGB-D), 3D Bounding Box (3D-BB), Scene Graph (SG), Voxel Map (VM) and NeRF. The tuning column outlines whether the vision model is finetuned during training (True/False). IF, ICL, R, and WK denote the *LLM Abilities* of Instruction-following, In-Context Learning, Reasoning, and World Knowledge. The *Fine-tuning* column summarizes how LLM components are fine-tuned, such as Prompt Tuning (PT), Low-Rank Adaptation (LoRA), Adaptive Fine-tuning (AF), Layer Freezing (LF), or Full Fine-tuning (Full). The *Hardware* column shows methods that are trained either with numbers of Nvidia GPU and the specific GPU type or with no training involved.

shape. ChatGPT also generates semantic part names and pairwise mappings (*e.g.* arm  $\rightarrow$  wing). A 3D segmenter then segments shapes based on semantic regions, utilizing the part mappings to produce sparse correspondence maps.

The knowledge-enhanced strategies described above enable strong performance especially in zero-shot scenarios where no labeled 3D data is available for a particular object or scene type. This allows open-ended reasoning about object parts, relationships, and semantics beyond fixed ontologies, as demonstrated by (i) Chen *et al.* [274] generating spatial and semantic object descriptions, (ii) ViewRefer [20] describing multi-view object relationships, and (iii) Abdelreheem *et al.* [22] generating and matching object part semantics across shapes.

#### 4.2.2 Reasoning-enhanced approaches

Along with world knowledge, the reasoning abilities of LLMs also help tackle other 3D tasks, particularly visual grounding in complicated 3D scenes with detailed geometry and multiple objects. In such cases, text descriptions of the objects should include their appearance and spatial relationship with surrounding items. Ordinary grounding methods [287] often struggle in this setting due to their inability to understand detailed text descriptions. LLM-Grounder [21], Transcribe3D [23], and zero-shot 3DVG [16] approach this problem by leveraging the reasoning capability of LLMs to analyze the text descriptions and generate a sequence of instructions for locating the objects using existing grounding

toolboxes. Specifically, an LLM first identifies anchor and target objects from the text descriptions. It then analyzes the spatial relationship (or described attributes) between multiple candidate objects based on their coordinates returned by the grounding tool to select the candidate that best matches the text description. In addition, (i) Transcribe3D [23] and LLM-Grounder [21] employ a multi-round interactive question-and-answer process to help users clarify their intentions, prompting them to provide instructions with more information to arrive at more accurate results, whereas (ii) LLM-Grounder includes multiple grounding tool choices, such as OpenScene [29] or LERF [30] to accommodate different 3D representations like point clouds or NeRF. A common drawback of these approaches is the “blindness” of the LLM since it is provided only with abstract textual descriptions of the 3D scene instead of the original point cloud of the scene. This may lead to the loss of crucial scene details. Consequently, when a 3D scene contains multiple objects of the same class, the absence of necessary scene details means that ambiguities of the text-based references cannot be resolved, which limits overall performance.

Besides visual grounding, the reasoning capability of LLMs facilitates other tasks as well. 3DAP [273] leverages GPT-4V to infer 3D information of an object from its 2D images using a visual prompting technique, where it annotates the input image with a 3D axis to enhance the LLM’s awareness of the 3D scale. ConceptFusion [18] uses GPT3 to generate instructions using pre-defined elementary spatial comparison modules to enable more

Method	Object Captioning	Scene Captioning	Dense Captioning	Grounding	QA	Situated QA	Dialogue	Planning	Navigation	Manipulation
3D-LLM [153]	✓	✓		✓	✓		✓	✓	✓	
Chat-3D [171]	✓				✓					
LEO [270]	✓	✓			✓	✓	✓	✓	✓	✓
LL3DA [19]	✓	✓	✓		✓		✓	✓		
PointLLM [267]	✓				✓		✓			
GPT4Point [268]	✓				✓		✓			
Chat-3D V2 [172]	✓	✓	✓	✓	✓					
LiDAR-LLM [271]	✓	✓		✓	✓	✓		✓	✓	
3DMIT [269]	✓	✓		✓	✓		✓			
MultiPLY [24]	✓				✓	✓	✓		✓	
3D-VLA [276]	✓		✓	✓	✓	✓		✓		✓
Agent3D-Zero [17]		✓		✓	✓		✓	✓	✓	✓
Scene-LLM [266]	✓		✓		✓		✓	✓		

TABLE 2: **Comparison of tasks** included in various 3D multi-task learning methods. QA stands for Question Answering. The methods are sorted chronologically from top (oldest) to bottom (most recent).

complex spatial reasoning using their proposed 3D feature map.

### 4.3 LLMs for 3D Multi-Task Learning

Many works focus on using the instruction-following and in-context learning capabilities of LLMs to unify multiple 3D tasks into a single language space. By employing different text prompts to denote different tasks, these studies aim for LLMs to serve as a unifying dialogue interface. Achieving multi-task learning using an LLM typically involves several key steps, beginning with the construction of 3D-text data pairs [19, 153, 270]. These pairs require crafting task instructions in text form and defining the output for each different task. Next, 3D data (typically in the form of point clouds) are fed into 3D encoders [288, 34] to extract 3D features. Alignment modules [171, 153, 172, 266] are subsequently used to (i) align 3D features with text embeddings from the LLMs across multiple levels (object-level, relationship-level, and scene-level) and (ii) translate the 3D features into tokens interpretable by the LLMs. Finally, an appropriate training strategy [272, 19, 153, 270, 269] needs to be selected, such as single or multi-stage 3D-language alignment training and multi-task instruction fine-tuning.

In the remainder of this section, we explore these aspects in detail. We additionally summarize the scope and capabilities of each method reviewed in this section in Table 2.

#### 4.3.1 Data for Multi-Task Learning

As demonstrated in Table 2, we divide tasks into four categories: captioning, grounding, question answering (QA), and embodied agent tasks (*i.e.*, planning, navigation, and manipulation). Accordingly, each task’s textual output follows a predefined format. For captioning and QA tasks, the output is plain text and is not constrained by a specific format. The output of the grounding task is a 3D bounding box, typically the coordinates of the referred object’s center along with its 3D size. Normally, the values for point and size are normalized to fall within the range of 0-255 [19] which limits the range of tokens the LLM is required to predict. For planning, the model outputs a series of steps to execute a task in text form, whereas for navigation, the output is a series of spatial coordinates. For manipulation, the output is action sequences in text form. Existing methods follow these guidelines to construct their multi-task instruction fine-tuning datasets.

Once the text format has been decided upon, different methods use different strategies to obtain text annotations for their datasets. Several approaches utilize human labelers to generate ‘ground truth’ annotations for each sample [218, 228, 234, 233], however this can be an expensive and time-consuming process. Another approach is to use ChatGPT [286] to generate text annotations for each sample, which is a strategy utilized by 3DMIT [269], LiDAR-LLM [271], Chat-3D [171] and Chat-3D v2 [172]. Here, 3D scene data is converted into text (usually by describing object bounding boxes and spatial relations textually), and a task description is created to describe the desired output. To guide ChatGPT towards the expected output format for the task, demonstration examples are provided, which allows ChatGPT to perform in-context learning to generate plausible text annotations for other 3D scenes. Alternatively, other multi-task datasets [19, 266] are constructed simply by merging existing 3D Vision-Language (VL) datasets [218, 228, 234, 153]. Some multi-task datasets are constructed using a combination of these three approaches, as seen in LEO [270], LiDAR-LLM [271] and 3D-LLM [153], seeking to combine the accuracy of human annotations with the scalability provided by using LLM-generated annotations.

#### 4.3.2 Training an LLM for multiple 3D tasks

The first step in training an LLM for multiple 3D tasks involves obtaining meaningful 3D features, where the extraction method varies depending on the type of 3D scene. For individual object point clouds, Point-LLM [267], Chat-3D [171], and GPT4Point [268] utilize Point-BERT [288] to extract 3D object features. For indoor scenes, LEO [270] uses PointNet++ [34] for feature extraction, whereas Chat-3D v2 [172] and 3DMIT [269] segment the scene and use Uni-3D [289] to extract features for each segmented part. Meanwhile, MultiPLY [24] integrates the extracted object features into a scene graph [290] to represent the entire scene. 3D-LLM [153] and Scene-LLM [266] lift features from 2D multi-view images into a 3D representation. 3D-LLM [153] lifts 2D semantic features from Mask2Former [291] or SAM [211]. Scene-LLM [266] follows ConceptFusion [18] to fuse both global information and local details, mapping pixel-wise CLIP features into point-wise 3D features. For outdoor 3D scenes, LiDAR-LLM [271] uses VoxelNet [292] to extract 3D voxel features.

For alignment modules, as discussed in Sec. 4.1, various network architectures are used. Notably, MultiPLY [24] employs distinct linear layers to align features from each modality. Chat-3D [171] and Chat-3D v2 [172] use a one-layer vanilla transformer to allow 3D object features to attend to each other during alignment. LEO [270] and LiDAR-LLM [271] utilize modified transformers as their alignment modules to better suit different types of 3D data (dense point clouds vs. sparse LiDAR). LEO [270] modifies the self-attention mechanism to explicitly encode spatial relations between object pairs in point clouds. In contrast, LiDAR-LLM [271] employs both self-attention and cross-attention mechanisms to align Bird’s Eye View (BEV) features with text features. 3D-LLM [153] and GPT4Point [268] adopt Q-Former, while LL3DA [19] adds an additional branch on top of Q-Former that allows query tokens to interact with visual prompts provided by users.

LLMs can be fine-tuned to incorporate multiple 3D tasks using different strategies discussed in Sec. 2.2.3. LEO [270], and 3DMIT [269] use low-rank adaptation (LoRA) for fine-tuning. As a result, the total trainable parameters, including those of alignment modules and 3D encoders, amount to less than 10% of the original LLMs’ parameters, significantly enhancing training efficiency. Chat-3D [171], LL3DA [19], Chat-3D v2 [172], LiDAR-LLM [271], and MultiPLY [24] adopt adaptive fine-tuning. Specifically, these models include modules that align spatial information in 3D scenes with language, *e.g.* a transformer layer, to capture object relationships. These modules, along with the pre-trained 3D encoders and LLMs, are fine-tuned for alignment. 3D-LLM [153], Scene-LLM [266], Point-LLM [267], and GPT4Point [268] employ layer freezing. By freezing most LLM layers and fine-tuning certain layers like the embedding layer, this strategy preserves linguistic capabilities while improving 3D understanding. Lastly, Agent3D-Zero [17] uses prompt tuning, a training-free method for guiding LLMs toward 3D task comprehension. This approach utilizes tailored prompts, adding grid lines and tick marks onto a BEV image of 3D scene, which help the 2D VLMs understand the 3D geometry.

Training these models for 3D multi-task learning also involves fine-tuning for *3D-language feature alignment*. Point-LLM [267], 3D-LLM [153], Scene-LLM [266], LEO [270], and GPT4Point [268] all adopt single-stage alignment methods. Specifically, Point-LLM [267] trains an MLP using only captioning data and additionally updates the input embedding layer to accommodate newly added tokens marking the start and end of point cloud tokens with ( $\langle p\_start \rangle$ ,  $\langle p\_end \rangle$ ). 3D-LLM [153] uses a custom dataset to train the alignment module along with the input and output embedding layers updating weights for newly added location tokens. Scene-LLM [266] trains only a linear layer to enable LLMs to understand both ego-centric and scene-centric perspectives using 3D frame-language pair caption tasks in camera and world coordinate systems. It also updates the input embedding layer to accommodate newly added tokens marking the start and end of 3D tokens ( $\langle 3D \rangle$ ,  $\langle /3D \rangle$ ). LEO [270] also trains the alignment modules using captioning tasks, but uniquely collects three types of captioning data: object-level [293], object-in-the-scene [228, 294], and scene-level [295], training its alignment module with all three datasets. GPT4Point [268] follows the structure and training strategy of BLIP2 [195], achieving alignment through three tasks: Point-Text Contrast (PTC), Point-Text Matching (PTM), and Point Caption Generation (PTG).

In contrast to these single-stage alignment methods, LiDAR-

LLM [271], Chat-3D [171], and Chat-3D v2 [172] each employ a 2-stage 3D-language alignment process. LiDAR-LLM [271] focuses on enhancing both local and global scene perception through 3D captioning tasks in two phases: first, concentrating on single-view captions and then expanding to panoramic scene descriptions. They develop instance-level perception capabilities through a blend of captioning and grounding tasks. Chat-3D [171] first aligns 3D objects with text using datasets for 3D object classification [296, 293, 297] aiming to maximize the cosine similarity between mapped 3D object features and object category word embeddings by updating only the alignment module. In the second stage of scene-level alignment, it utilizes ScanRefer [218] to enable captioning capabilities, updating an additional transformer layer specifically to model spatial relationships of objects. Similarly, Chat-3D v2 [172] incorporates object-level and scene-level alignments, with the second stage additionally training a position embedding layer. For training efficiency, both LL3DA [19] and 3DMIT [269] skip the alignment stages and focus solely on the stage of instruction tuning described below.

Nearly all multitask learning methods ultimately require the ability to complete various 3D tasks based on instructions. Thus, as the final stage of training, each method typically uses their own constructed multitask instruction-following dataset for instruction fine-tuning<sup>1</sup>. Since all task outputs are unified into textual form, the training loss used is the standard autoregressive loss used in LLMs. This stage usually involves jointly training the alignment module and the LLM. An exception is Agent3D-Zero [17], which completes various 3D tasks by feeding GPT4V with 2D images from different viewpoints, thus it does not require any training.

#### 4.4 LLMs as 3D Multi-Modal Interfaces

In addition to exploring 3D multi-task learners, some recent studies incorporate information across different modalities to further improve the capability of the models and enable novel interactions. Apart from text and 3D scenes, multi-modal 3D-LLMs may also include 2D images, audio, or touch information in scenes as inputs.

Most works aim to construct a common representation space across different modalities. Since several existing works [299, 300] have already provided pre-trained encoders that map text, images, or audio to common spaces, some works choose to learn a 3D encoder that aligns 3D embeddings to the embedding space of pre-trained encoders for other modalities. JM3D-LLM [279] learns a 3D point cloud encoder that aligns the embedding space of the point cloud to the text-image embedding space of SLIP [301]. It renders a sequence of images of the point cloud and constructs a hierarchical text tree during training to enable a detailed alignment. Point-Bind [272] also learns a similar 3D encoder and aligns it to ImageBind [302] to unify the embedding space of images, text, audio, and point clouds. This enables tackling different tasks such as retrieval, classification, and generation among the various modalities using different task heads. However, one notable limitation is that this approach only works on small-scale object-level scenes as it is computationally expensive for a 3D encoder to process a large scene with millions of points. Moreover, most pre-trained multi-modal encoders like CLIP are designed for single-object scenes and are not suitable for large scenes with multiple objects and local details.

1. Instruction fine-tuning refers to the process of further fine-tuning LLMs on a dataset consisting of (INSTRUCTION, OUTPUT) pairs [298]

Large scenes instead require more meticulous design to incorporate multiple modalities. ConceptFusion [18] constructs an enhanced feature map that fuses both global information and local details for each constituent image of a large scene. This is achieved by using pre-trained feature extractors [187, 188] that have already been aligned to different modalities including text and audio. It then maps the feature maps to the point cloud of the scene using traditional SLAM approaches. MultiPLY [24] adopts a similar representation to ConceptGraph [290]. It identifies all salient objects in the scene, obtains the global embedding for each object, and finally constructs a scene graph. The resultant representation is a scene embedding aligned with the embedding space of Llama [140]. The embeddings of other modalities including audio, temperature, and sense of touch can also be mapped to the same space using linear projection. All embeddings are tokenized and sent to the LLM at once. Compared with methods on object-level scenes, approaches that can process large scenes reduce costs by relying on pre-trained encoders to bridge the modality gap, instead of learning new ones from scratch.

## 4.5 LLMs for Embodied Agents

3D embodied agents can be created using the planning, tool-using, and decision-making abilities of LLMs. Such abilities enable LLMs to generate intelligent decisions that encompass navigation within a 3D environment [270, 275, 11], interaction with objects [14], and selecting the appropriate tools to execute specific tasks [24]. This section describes how 3D embodied agents perform the tasks of planning, navigation, and manipulation.

### 4.5.1 3D Task Planning

For embodied agents, ‘task planning’ refers to the ability to generate steps to execute a specific task, given the task description and the 3D environment. Task planning usually serves as a prerequisite for navigation and manipulation tasks [12, 275] as the accuracy of planning directly influences the performance of subsequent tasks.

LEO [270] and LLM-Planner [12] utilize LLMs to generate step-by-step plans which they adjust dynamically based on environmental perceptions. LEO [270] emphasizes scene-aware planning grounded in the current scene’s configurations, whereas LLM-Planner [12] adopts GPT3 [127] to divide planning into high-level subgoals and low-level actions, and replan when the agent gets stuck during task execution. 3D-VLA [276] integrates 3D perception, reasoning, and action through a generative world model. It focuses on enhancing planning capabilities by utilizing its generative model to predict future state representations (*e.g.* goal images and point clouds). Agent3D-Zero [17] introduces Set-of-Line Prompting (SoLP) that enhances the VLM’s comprehension of the scene’s geometric aspects by generating diverse observational viewpoints. Specifically, SoLP superimposes grid lines and tick marks onto BEV images, and prompts the VLM to provide more accurate camera positions and orientations, which enables the task of the VLM to understand 3D spatial concepts. UniHSI [277] addresses the task of Human-Scene Interaction (HSI), which involves generating interactions between humans and objects within 3D environments based on input language commands. It uses an LLM as a planner to translate language commands into task plans represented as Chains of Contacts (CoC), a sequence that represents the chronological relationships between human joint points and object positions. While the aforementioned

approaches focus on planning within a single scene, SayPlan [275] can handle multiple rooms and floors by (i) leveraging 3D scene graphs for semantic search and (ii) integrating classical path planning with an iterative replanning pipeline for plan refinement.

### 4.5.2 3D Navigation

3D Navigation refers to the ability of an embodied agent to move and orient itself within 3D environments, often based on visual inputs and language instructions. Each of the described methods – LEO [270], Agent3D-Zero [17], LLM-Planner [12], and NaviLLM [11] – implements 3D navigation in different ways. LEO [270] processes egocentric 2D images and object-centric 3D point clouds alongside textual instructions. It generates a sequence of action tokens that correspond to executable navigation commands like ‘move forward’ or ‘turn right’. LEO employs ‘shortest path navigation trials’, which provide a less noisy and more straightforward learning environment compared to human demonstrations. Agent3D-Zero [17] navigates by continuously selecting new viewpoints based on assessments of the environment. It incorporates historical data from previous viewpoints to refine its navigation path towards specific goals, such as finding a printer in an office setting. LLM-Planner [12] employs a hierarchical approach, that first generates high-level plans as sequences of subgoals, which are then translated into a series of primitive actions by a low-level planner. This makes the overall process adaptable to the immediate environment. NaviLLM [11] transforms various embodied navigation tasks into generation problems using schema-based instructions. These instructions include 4 elements: a task defined by a word sequence, observations of all reachable viewpoints, the history of past visual observations, and output hints that guide action generation (*e.g.* selecting a direction or object).

### 4.5.3 3D Object Manipulation

Manipulation in the context of 3D embodied agents refers to their ability to physically interact with objects, ranging from moving objects to complex sequences such as assembling parts or opening doors. The core idea used to enable LLMs to perform manipulation tasks lies in tokenizing action sequences. To let LLMs output specific actions, it is first necessary to define action tokens that allow LLMs to generate said actions, based on the task and 3D scene context. Subsequently, platforms like CLIPort [242] or motion planning modules in robot arms translate these tokenized actions into physical movements to be executed by the agent.

LEO [270], MultiPLY [24], and 3D-VLA [276] each use different action tokens to convert spoken or written instructions into actions for robots in 3D spaces. LEO [270] uses more than 500 specific tokens to make robot movements precise. Specifically, for the CLIPort [242] task, action poses are encoded using 516 tokens: 320 tokens for the x-axis pose bins, 160 tokens for the y-axis, and 36 tokens for z-rotation bins. MultiPLY [24] extends this by introducing tokens like ⟨SELECT⟩ for object interaction, ⟨NAVIGATE⟩ for movement, ⟨OBSERVE⟩ for scrutiny, ⟨TOUCH⟩ for tactile feedback, ⟨HIT⟩ for auditory feedback, ⟨PICK-UP⟩ and ⟨PUT-DOWN⟩ for manipulation, and ⟨LOOK-AROUND⟩ for awareness. This approach also integrates sensory feedbacks (tactile, temperature, and auditory) which enhances the interaction of the robot with its surroundings. 3D-VLA [276] incorporates (i) object tokens (⟨obj⟩/⟨obj⟩) to identify manipulated objects, (ii) location tokens (⟨loc0-255⟩) for spatial grounding,

and (iii) specialized tokens for robotic actions like arm location/rotation/gripper state. These tokens are separated by  $\langle \text{ACT SEP} \rangle$ . This token structure enables understanding and executing complex 3D manipulation.

While these systems enable robots to perform complex tasks by mapping instructions to actions, they overlook semantic understanding of manipulable objects and are often unable to distinguish between suitable and unsuitable parts for manipulation. To address this issue, VoxPoser [13], LAN-grasp [14], and ManipLLM [15] focus on “affordance”, and create affordance maps to represent objects and features in their surroundings that can be utilized to perform specific tasks, such as graspable handles [14, 15], pressable buttons [15], or movable objects [13]. Specifically, VoxPoser [13] uses an LLM to decompose free-form language instructions, infer affordances and constraints, and compose 3D voxel maps by interacting with VLMs using code interfaces. These maps enable generating closed-loop robot trajectories that are robust to dynamic changes, with capability to learn from online experiences in contact-rich environments. LAN-grasp [14] employs foundation models to deepen robots’ understanding of objects for semantically appropriate grasping by combining multiple models to identify graspable parts, without the need for retraining. ManipLLM [15] predicts manipulation outcomes by identifying 3D coordinates for contact points and gripper orientations from text prompts, RGB images, and depth maps.

## 4.6 LLMs for 3D Generation

Traditionally, 3D modeling has been a complex time-intensive process with a high barrier to entry, requiring detailed attention to geometry, texture, and lighting to achieve realistic results. In this section, we scrutinize the integration of LLMs with 3D generative techniques, where we show how language provides a way to generate contextualized objects in scenes and provides innovative solutions to 3D content creation and manipulation.

### 4.6.1 Object-level Generation

Shape-GPT [283] quantizes 3D shapes into discrete “shape word” tokens using a shape-specific 3D VQ-VAE. This enables the integration of shape data into a multi-modal input for the T5 language model [139] along with text and images. This multi-modal representation enables T5 to learn cross-modal interactions for, *e.g.* text-to-shape generation and shape editing/completion. GPT4Point [268] uses a two-stream approach - aligning point cloud geometry with text via Point-QFormer, which then feeds into coupled LLM and diffusion paths for text comprehension and high-fidelity 3D object generation conforming to text input.

In contrast, MeshGPT [282] and PolyGen [280] do not condition the generation on text, but they still adopt an autoregressive approach akin to sequence modelling in LLMs. MeshGPT uses graph convolutions to encode mesh geometry/topology into rich embeddings compressed via Residual Vector Quantization and fed into a GPT-style transformer to autoregressively predict tokens/embeddings for generating meshes with desired properties. PolyGen [280] is an autoregressive transformer-based model of 3D meshes, which utilizes pointer networks. It consists of a vertex model that unconditionally models mesh vertices, and a face model for mesh faces conditioned on input vertices using autoregressive networks to output face indices and vertex coordinates for generating diverse high-quality meshes.

### 4.6.2 Scene-scale Generation

Holodeck [284] and GALA-3D [25] employ multi-stage pipelines to progressively refine an initial coarse 3D scene layout from text into a detailed realistic 3D environment. Holodeck employs specialized modules to craft a basic layout, select materials, and incorporate elements like doors and windows based on GPT-4’s spatial reasoning and placement/style suggestions. It then populates the layout with Objaverse assets matched to GPT-4’s textual descriptions. An optimizer arranges these objects adhering to spatial relational constraints obtained from GPT-4 encouraging realistic object layouts and interactions.

GALA-3D [25] first generates coarse layouts from text using an LLM, then translates them into a 3D Gaussian representation. This representation serves as the foundation for creating detailed 3D content using instance-level text-to-image diffusion priors. It employs compositional optimization to fine-tune the parameters of the layout-guided Gaussians, ensuring the final scene aligns with the text for object placement, scale, and interaction.

Both leverage complementary strengths of LLMs to extract high-level semantic layouts and generative models/optimization to convert these into geometrically and physically plausible 3D scenes.

### 4.6.3 Procedural Generation and Manipulation

LLMR [281], 3D-GPT [26] and SceneCraft [303] adopt modular architectures with specialized components/agents for interactive 3D world creation and code generation from natural language. LLMR consists of distinct components for generating code to construct scenes in Unity, understanding existing scene objects and properties to enable modifications, identifying required functions to execute instructions, and evaluating final code quality. Similarly, 3D-GPT has components for interpreting instructions and determining required generation functions, enriching descriptions with detailed modeling attributes, and translating enriched descriptions to Python code for the Blender API. Overall, these methods showcase task decomposition and specialization of LLM components to handle instruction interpretation, function mapping, and robust code generation.

## 5 3D TASKS WITH VLMs

While Section 4 discussed methods integrating LLMs in 3D tasks, a vast body of research has explored various aspects of 3D understanding through the lens of 2D Vision-Language Models (VLMs). VLMs include much richer visual information that can be linked directly to 3D. This section reviews contributions from a series of recent papers covering language-driven open-world understanding, instance-level understanding, unified end-to-end architectures, spatial reasoning, generation, and beyond.

### 5.1 Open-Vocabulary 3D Scene Understanding

Open-vocabulary 3D scene understanding aims to recognize and describe scene elements using natural language descriptions instead of predefined category labels. OpenScene [29] takes a zero-shot approach by predicting dense features for 3D scene points that are co-embedded with CLIP’s text and image pixel embeddings in a shared feature space, enabling task-agnostic training and open-vocabulary querying to identify objects, materials, affordances, activities, and room types. CLIP-FO3D [304] follows a similar approach, modifying CLIP to extract dense pixel features from

3D scenes which are projected to point clouds, then training a 3D model via distillation to transfer CLIP’s knowledge. Semantic Abstraction [305] extracts relevancy maps from CLIP as abstracted object representations to generalize to novel semantics, vocabularies, and domains. Open-Fusion [306] combines the SEEM [307] vision-language model with TSDF 3D mapping for real-time open-vocabulary scene creation and querying, utilizing region-based embeddings and confidence maps.

Approaches such as PLA [308] and RegionPLC [309] leverage contrastive learning to combine captions with 2D and 3D data modalities to associate visual and semantic information. PLA [308] uses 3D-caption pairs and contrastive learning to associate multi-view images with captions for learning visual-semantic representations, while RegionPLC [309] proposes region-aware contrastive learning by combining region-level captions from 2D models mapped to 3D points. OVIR-3D [310] fuses 2D region proposals and text-aligned features from an off-the-shelf 2D detector into 3D instances for efficient open-vocab retrieval. CoDA [311] uses 3D geometry priors from annotated base categories and CLIP’s 2D semantic priors in its 3D Novel Object Discovery (3D-NOD) strategy. Its Discovery-driven Cross-Modal Alignment (DCMA) aligns 3D and image/text features for novel object localization and classification.

Instance-level scene understanding works such as OpenMask3D [312] and Open3DIS [313] utilize predicted class-agnostic 3D instance masks and 2D segment-level CLIP embeddings to enable open-vocabulary 3D instance segmentation. OpenIns3D [314] achieves open-vocabulary understanding without aligned images, using a “Mask-Snap-Lookup” pipeline that predicts 3D mask proposals, generates synthetic scene images, and assigns categories to masks via a language module. Rozenberszki *et al.* [315] propose to leverage CLIP features to ground 3D feature learning for 3D semantic and instance segmentation.

Language grounding with NeRFs has shown promising results in open-vocabulary scene understanding. Several methods, such as DFF [316], LERF [30], VL-Fields [317], and 3D-OVS [318], distill the knowledge of 2D feature extractors like DINO or CLIP into 3D feature fields by minimizing the error of volume-rendered features with respect to the 2D features, enabling query-based local editing and grounding language into neural implicit representations. LERF [30] optimizes a dense, scale-conditioned 3D language field by volume rendering CLIP embeddings. LangSplat [319] and N2F2 [320] demonstrate efficient open-vocabulary querying and interaction within a 3D Gaussian Splatting representation by leveraging hierarchical supervision and multiscale feature fields.

## 5.2 Text-Driven 3D Generation

Section 4.6 covered methods that used LLMs for 3D generation. Here, we survey text-to-3D generation methods that leverage guidance from 2D VLMs [174] and text-to-image diffusion models [321, 322] using differentiable rendering. Early works such as DreamFields [323], CLIP-Mesh [32], CLIP-Forge [324] and Text2Mesh [325] explore zero-shot 3D generation guided by CLIP.

DreamFusion [31] introduced Score Distillation Sampling (SDS) where the parameters of a 3D representation are optimized by making its renderings from arbitrary perspectives appear highly realistic, as evaluated by a pre-trained 2D diffusion model. It uses the text-to-image Imagen model [322] to optimize a NeRF representation via SDS. Magic3D [326] proposes a two-stage framework: generating a coarse model with a low-resolution diffusion

prior and sparse 3D hash grid, then optimizing a textured 3D mesh model with an efficient differentiable renderer and high-resolution latent diffusion model [321]. Fantasia3D [327] disentangles geometry and appearance, using a hybrid DM Tet [328] representation and spatially varying BRDFs. ProlificDreamer [329] introduced Variational Score Distillation (VSD), a particle-based framework treating 3D parameters as random variables to improve fidelity and diversity. Dream3D [330] utilizes explicit 3D shape priors and text-to-image diffusion models for enhanced text-guided 3D synthesis. MVDream [331] employs a multi-view consistent diffusion model trainable on few-shot data for personalized generation. Text2NeRF [332] combines NeRF representations with pre-trained text-to-image diffusion models to generate diverse indoor/outdoor 3D scenes from language. Apart from simultaneously generating geometries and appearance, several studies explore the possibility of solely synthesizing the textures based on given geometries [333, 334, 335].

For human avatars, AvatarCraft [336] uses diffusion models to guide neural implicit field geometry/texture learning from text prompts. Additionally, it enables animating these human avatars by deforming the neural implicit field with an explicit warping field that maps the target human mesh to a template human mesh. AvatarCLIP [337] proposes a zero-shot CLIP-supervised framework for 3D avatar generation, geometry sculpting, texture mapping and motion synthesis from text. CG-HOI [338] uses diffusion models to characterize dynamic human-object interactions from text. GenZI [339] distills information about human interactions via a pre-trained vision-language model, producing zero-shot 3D human-scene interaction synthesis from text prompts.

Exploring compositional generation, CG3D [340] generates scalable 3D scenes using explicit 3D Gaussian radiance fields by compositing individual objects without bounding boxes. Po *et al.* [341] introduce locally conditioned diffusion for granular scene control via text prompts and bounding boxes. GraphDreamer [342] generates compositional scenes from scene graphs by decomposing them into global-local descriptions to optimize object SDFs.

Overall, these approaches combine diffusion models, vision-language models, neural representations, and 3D priors for text-to-3D generation of objects, avatars, and scenes.

## 5.3 End-to-End Architectures for 3D Vision & Language

Transformer models pre-trained on large 3D-text datasets learn powerful joint representations that bridge the visual and language modalities. 3D-VisTA [343] is a transformer model that employs self-attention to jointly model 3D visual and text data, enabling effective pre-training on objectives like masked language/object modeling and scene-text matching. UniT3D [227] takes a unified transformer approach, combining a PointGroup 3D detection backbone, BERT text encoder, and multi-modal fusion module, with joint pre-training on synthetically generated 3D-language data. SpatialVLM [344] takes a different tack, and co-trains VLMs on a large synthetic 3D spatial reasoning dataset, boosting performance on 3D spatial visual question answering tasks and enabling applications like chain-of-thought reasoning for robotics. Multi-CLIP [345] pre-trains a 3D scene encoder to align scene features with CLIP’s text and image embeddings, aiming to transfer CLIP’s knowledge for improved 3D understanding on tasks like visual question answering.

In addition to pre-training approaches, researchers have explored architectures that unify 3D perception with language capabilities in an end-to-end framework. D3Net [27] combines dense

captioning and visual grounding with a 3D object detector, a speaker for generating captions from detections, and a listener for discriminating objects using the captions. Uni3DL [28] operates on point clouds, with modules for text encoding, point encoding, semantic/mask prediction, and diverse task outputs like segmentation, detection, grounding, and captioning. InstanceRefer [346] uses panoptic segmentation and linguistic cues to filter instance candidates based on language descriptions for visual grounding tasks in 3D point clouds, while LanguageRefer [347] combines language embeddings with spatial embeddings from 3D bounding boxes. 3DVG-Transformer [348] also tackles 3D grounding in point clouds, with a coordinate-guided contextual aggregation module and multiplex attention for effective feature fusion.

## 6 DATASETS

We now provide a high-level overview of the datasets that are used to train and evaluate 3D vision-language models. In Table 3, we provide a list of datasets alongside the tasks they are used for, as well as information about the 3D scans and annotations. In Fig. 4, we present these datasets on a timeline, showing where each dataset sourced 3D information from. Current 3D vision-language datasets are almost exclusively generated by taking existing 3D vision datasets, and applying human, model or templated annotations to samples. As seen in Table 3, a majority of existing datasets focus on real, indoor scenes, and this is partially explained by observing that the majority of existing datasets use 3D scans from ScanNet [361] and 3RScan [295]. Many of the datasets presented here share the same 3D data, and instead differ primarily through their choice of annotation strategy, and the 3D vision-language task they are designed to be used for.

Datasets for 3D navigation and manipulation using language are often designed around specific requirements and have a large overlap with existing bodies of research. We refer readers to existing survey papers [362, 363] for an overview of these datasets. Similarly, for text-to-3D generation datasets, we direct readers to the recent survey by Lee *et al.* [243]. We omit further discussion here due to prior extensive coverage, and because many methods use 2D vision-language data rather than 3D-specific datasets.

**Cap3D** [349] is a 3D object captioning dataset developed upon 660k objects from the Objaverse [293] dataset. It is constructed by generating 2D image captions from multiple views of the 3D object, and consolidating those captions using image-text alignment and LLMs.

**Text2Shape** [350] is a human-captioned form of the 8,447 tables and 6,591 chairs found in ShapeNet [296], combined with a procedurally generated dataset of primitive shapes labeled with template-based captions. It was originally used for generative text-to-3D shape tasks.

**SceneVerse** [351] is a large-scale, multi-purpose dataset of annotated scenes made by compiling 68k scenes from existing 3D datasets. SceneVerse contains a total of 2.5 million vision-language pairs for object captioning, scene captioning and generating relative descriptions, primarily generated through the use of 3D scene graphs and LLMs.

**nu-Caption** [271] is a captioned version of 420k LiDAR scans from the nuScenes [364] dataset, annotated using GPT-4 and 2D MLLMs. Captions include general scene descriptions, detailed descriptions of objects and their relationships, and the identification of potential risks on the road.

**nu-Grounding** [271] builds on nu-Caption by focusing on the task of grounding, using the annotations from nuScenes to create 280k pairs of questions and answers for visual grounding and grounded captioning.

**ScanRefer** [218] introduces the task of 3D RGB-D grounding using a natural language expression by creating 51,583 human-annotated ‘referring expressions’ of 11,046 objects found in 800 scenes of ScanNet [361]. The input consists of a point cloud of a scanned 3D scene alongside a free-form description of a specified target object, and the output is the corresponding bounding box of the object. ScanRefer provides an evaluation server and online benchmark <sup>2</sup> to enable comparison between different methods.

**ReferIt3D** [228] introduces a number of datasets (Nr3D, Sr3D and Sr3D+) consisting of objects from 707 ScanNet scenes. Similarly to ScanRefer, these object have been annotated with referring expressions, with a focus on queries where the scene contains multiple instances of the target class, and the referring expression is required to disambiguate between them. Nr3D contains 41,503 human-annotated, free-form utterances to refer to objects in 3D scenes, Sr3D contains 83,572 template-based utterances, and SR3D+ is a version of Sr3D with augmented utterances. ReferIt3D also provides an evaluation server and online benchmark <sup>3</sup> to enable comparison between different methods.

**Multi3DRefer** [230] is a modified version of the ScanRefer dataset. Instead of referring expressions that always refer to one object in the scene, Multi3DRefer contains 6688 zero-target, 42,060 single target and 13178 multiple target referring descriptions collected for 11,609 objects in 800 ScanNet scenes. ChatGPT [286] is also used to rephrase the referring expressions.

**Chat-3D v2** [172] is another modified form of ScanRefer, where the referring expressions from 705 scenes in ScanNet are used to construct scene captions that describe the relationships between objects in the scene. The scene captions are generated using GPT-4 [365] by providing the model with ground-truth information about objects. The generated captions contain references to explicit ‘object identifiers’ that directly represent each object in the scene.

**EmbodiedScan** [352] is an annotated combination of Matterport3D [285], 3RScan [295] and ScanNet [361], designed as a multi-modal, ego-centric dataset for 3D scene understanding. Segment Anything [366] and other annotation tools are used to provide 3D bounding boxes, semantic occupancy, and 970k template-based language descriptions across a total of 5185 scenes.

**ScanEnts3D** [353] extends both ScanRefer [218] and ReferIt3D [228] by using professional annotators to link every object mentioned in referential sentences to their respective instances within a 3D scene. In the original paper this dataset is only used for training purposes, where it is found to improve the model’s performance on other visual grounding and captioning datasets.

**WildRefer** [354] presents the STRefer and LifeRefer datasets, emphasizing human-centric *in the wild* settings with comprehensive 3D and linguistic human-annotations for 3D grounding. STRefer contains 5,458 referring expressions for objects in 662 scenes from the STCrowd [367] dataset, whereas LifeRefer contains 25,380 referring expressions for objects in 3,172 scenes from a new set of 3D scans acquired for this dataset.

**RIORefer** [355] is a human-annotated version of 3RScan [295], used for 3D grounding. It consists of 63k

2. [https://kaldir.vc.in.tum.de/scanrefer\\_benchmark/](https://kaldir.vc.in.tum.de/scanrefer_benchmark/)

3. <https://referit3d.github.io/benchmarks.html>

Dataset	Object Captioning	Scene Captioning	Dense Captioning	Single Object Grounding	Multiple Object Grounding	Question Answering	Situated Question Answering	Dialogue	Task Planning	Real	Synthetic	Object	Indoor	Outdoor	Human-Annotated	Model-Annotated	Template-Based
Cap3D [349]	✓								✓	✓	✓				✓		
Text2Shape [350]	✓									✓	✓				✓		✓
SceneVerse [351]	✓	✓		✓					✓	✓		✓			✓	✓	✓
nu-Caption [271]		✓							✓				✓		✓		✓
nu-Grounding [271]		✓		✓					✓				✓		✓		✓
ScanRefer [218]			✓	✓					✓			✓			✓		
ReferIt3D [228]			✓	✓					✓			✓			✓		✓
Multi3DRefer [230]			✓		✓				✓			✓			✓	✓	
Chat-3D v2 [172]	✓			✓					✓			✓					✓
EmbodiedScan [352]				✓					✓			✓				✓	✓
ScanEnts3D [353]			✓	✓					✓			✓			✓		
WildRefer [354]				✓					✓			✓	✓		✓		
RIORefer [355]				✓					✓			✓			✓		
ARKitSceneRefer [356]				✓					✓			✓			✓	✓	
ScanERU [229]				✓					✓	✓		✓			✓		
DenseGrounding [231]					✓				✓			✓			✓		
ScanQA (Azuma <i>et al.</i> ) [234]						✓			✓			✓			✓		
ScanQA (Ye <i>et al.</i> ) [357]						✓			✓			✓			✓		
3DMV-VQA [236]						✓			✓			✓					✓
NuScenes-QA [235]						✓			✓				✓				✓
CLEVR3D [358]						✓			✓	✓		✓					✓
SQA-3D [233]							✓		✓			✓			✓		
3D-LLM [153]	✓	✓	✓	✓		✓	✓	✓	✓			✓				✓	
ScanScribe [294]			✓	✓		✓	✓		✓	✓		✓			✓	✓	✓
M3DBench [359]		✓	✓	✓	✓	✓	✓	✓	✓			✓			✓	✓	✓
GPT4Point [268]	✓					✓	✓		✓	✓	✓					✓	
LAMM [360]	✓	✓				✓	✓		✓	✓	✓	✓	✓			✓	✓

TABLE 3: **An overview of datasets** used for 3D-Related tasks using Large Language Models. For each dataset, we show which tasks that dataset has been used to demonstrate, whether the data is captured from the real world or synthetically generated, whether the 3D data is of an object, an indoor scene or an outdoor scene, and how the annotations are obtained. We focus primarily on newer datasets which are used to evaluate methods in recent research papers.

descriptions of objects across 1,380 scenes. This dataset is introduced as a way of testing the cross-dataset generalization abilities of models, such as in the proposed ‘‘ScanRefer to RIORefer generalization’’ and ‘‘RIORefer to ScanRefer generalization’’ tasks.

**ARKitSceneRefer** [356] is an annotated version of ARKitScenes [368] emphasizing the 3D grounding of small, everyday objects found in real-world indoor environments. It contains 15k descriptions of objects found in 1,605 scenes.

**ScanERU** [229] is a modified and human-annotated version of ScanNet that combines 46k referring expressions from ScanRefer with 706 ScanNet scenes that have been modified to include a 3D human model gesturing to the referred object, using locations designated by human annotators.

**DenseGrounding** [231], like Multi3DRefer, seeks to extend

the task of 3D grounding to include multiple objects, however instead of a single referring expression referring to multiple objects, each input is a combined paragraph of referring queries which each correspond to a single object. These paragraphs are constructed using the nearest neighbors of random objects from ScanRefer and ReferIt3D, and combining their referring expressions together to form a paragraph.

**ScanQA (Azuma *et al.*)** [234] is an annotated version of ScanNet with 41k question-answer pairs generated across 800 scenes. Questions are automatically generated using the referring expressions in ScanRefer and then refined by human annotators, whereas answers are derived entirely from human-annotators. This is the dataset that is typically referred to by the name ‘‘ScanQA’’.

**ScanQA (Ye *et al.*)** [357] was released contemporaneously with ScanQA (Azuma *et al.*) and is also a human-annotated form

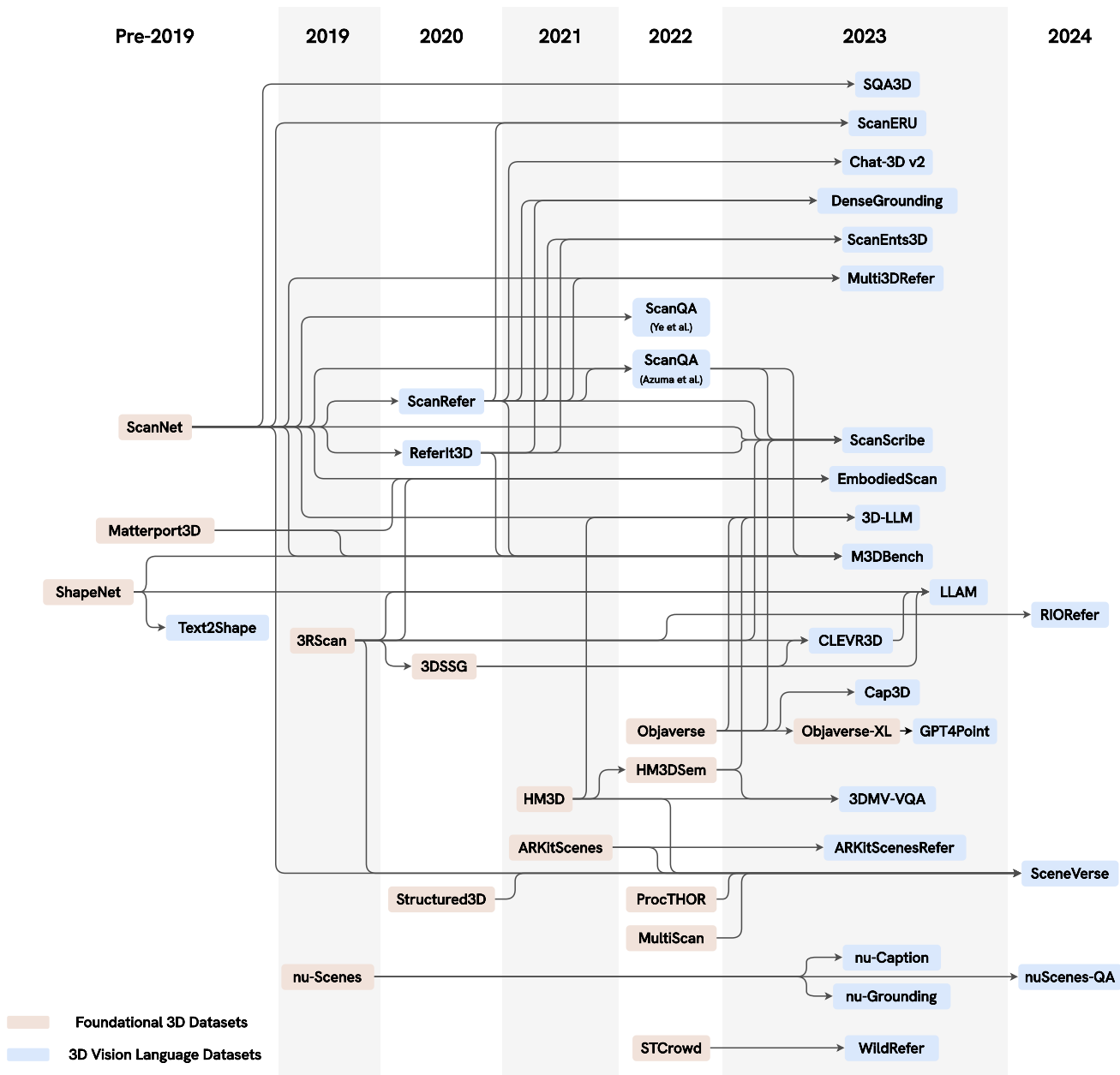


Fig. 4: **Timeline of datasets.** A timeline showing how existing datasets are combined and annotated to form new datasets for 3D vision language tasks. Datasets in orange are foundational 3D datasets without language annotations and datasets in blue are the annotated datasets used in 3D vision language tasks. Many existing datasets use 3D data from the same sources, such as ScanNet and 3RScan, and instead differ primarily through their choice of annotation strategy and targeted 3D vision task. Note that WildRefer also introduces new 3D data and annotations for vision-language tasks.

of ScanNet to be used as a 3D question answering dataset. Ye *et al.* contains 10k question-answer pairs for 806 ScanNet scenes. While Azuma *et al.* initially generates questions using referring expressions from ScanRefer, Ye *et al.* use human annotators for the entirety of question creation.

**3DMV-VQA** [236] is an annotated version of 5k scenes from the Habitat-Matterport 3D Dataset (HM3D) [369], using the semantic information from HM3DSem [370] to generate 50k questions of four types: “concept”, “counting”, “relation” and “comparison”. These questions are generated as templates, and then transformed into natural language questions.

**NuScenes-QA** [235] consists of 34k scenes from

nuScenes [364] annotated with 460k template-style question-answer pairs generated using a constructed scene graph. Questions are divided into 5 types: “existence”, “counting”, “query-object”, “query-status” and “comparison”, and can include spatial reasoning.

**CLEVR3D** [358] is an annotated form of 3RScan [295] designed for indoor 3D QA tasks. Template-based questions and answers are generated using the scene graph annotations from 3DSSG [371]. Initially, 44k questions are generated for 1,333 scenes, however they use a “compositional scene manipulation” technique to randomly replace objects in the scene graphs with objects from a generated object pool, artificially leading to 171k

questions across 8,771 scenes.

**SQA-3D** [233] is another human-annotated version of ScanNet, proposing the problem of “situated question answering”, where each query consists of a description of the agent’s current location and situation, and a query relating to the scene. SQA-3D contains 33.4k questions across 650 scenes.

**3D-LLM** [153] is an annotated version of Objaverse, ScanNet and HM3D/HM3DSem designed to handle a broad variety of tasks involving 3D vision and language. BLIP-2 [195] and ChatGPT [286] are used to generate 300k instances of ‘3D-language data’ that are used across a range of 3D vision-language tasks.

**ScanScribe** [294] is an annotated version 1,185 scenes from ScanNet and 3RScan designed to act as a large-scale 3D scene-text pair dataset for pre-training 3D vision-language models. It utilizes ScanQA, ScanRefer and ReferIt3D for ScanNet data, and uses GPT-3 prompting to generate annotations for 3RScan to create a total of 278k scene descriptions. To increase the diversity of the dataset, scenes are synthetically generated by random replacing 10% of the objects in scenes with a same-category object from Objaverse.

**M3DBench** [359] is a multi-modal instruction-following dataset consisting of 327k instruction-response pairs across a broad range of tasks. Data is collected from a large set of existing datasets (see Fig. 4), alongside using GPT-prompting to generate additional annotations.

**GPT4Point** [268] is an annotated form of over 1 million objects from Objaverse-XL, designed for 3D Captioning, 3D QA and other 3D tasks. Annotations are generated automatically through a hierarchical pipeline that fuses and improves captions from multiple views.

**LAMM** [360] is a large scale multi-modal instruction-tuning dataset that covers tasks for both 2D and 3D vision. The 3D Data is sourced from 3RScan [295], CLEVR3D [358], 3DSSG [371] and ShapeNet [296], and is annotated using GPT [365] and template-based responses.

## 7 CHALLENGES AND OPPORTUNITIES

Despite progress in integrating LLMs with 3D data, challenges remain in data representation, computational efficiency, and benchmarks, necessitating innovative solutions.

**Representation Choice** has a large impact on the performance of 3D vision language models. Currently, point clouds are predominantly used to represent both indoor (*e.g.* vertices of meshes) and outdoor (*e.g.* LiDAR point clouds) environments due to their simplicity and neural network compatibility. However, they struggle to capture the fine details crucial for accurate, rich spatial models. Developing novel 3D scene representations that more effectively bridge the gap between spatial information and language could unlock new levels of understanding and interaction. By finding innovative ways to encode language and semantic information in 3D representations, such as using distilled language and semantic embeddings [30, 316], could help bridge the gap between these two modalities.

**Computational Demands** of both 3D data processing and LLMs pose significant challenges. Scalability remains a concern as the complexity of 3D environments and the size of language models increase. Advances in LLM architectures designed for adaptivity and computational efficiency could significantly broaden their

application scope.

**Improving Benchmarks** is essential for comprehensively evaluating and advancing the capabilities of multi-modal LLMs in 3D tasks. Current benchmarks have limited scope, especially regarding 3D reasoning, hampering evaluation of spatial reasoning skills as well as development of 3D decision-making/interaction systems. Moreover, the metrics in use today fall short of capturing the full spectrum of LLMs’ capabilities in 3D environments. Crafting task-specific metrics that more precisely measure performance across diverse 3D tasks is essential. Finally, the granularity of current scene understanding benchmarks is overly simple, limiting insight into complex 3D environment comprehension. A more diverse array of tasks is required.

**Safety and Ethical Implications** are imperative to consider when employing LLMs for 3D understanding. LLMs can hallucinate and output inaccurate, unsafe information leading to erroneous decisions in critical 3D applications. Moreover, LLMs often fail in ways that are unpredictable and challenging to interpret. They may also inherit societal biases present in training data, disproportionately disadvantaging certain groups when making predictions in real-world 3D scenes. It is crucial to approach the use of LLMs in 3D contexts with caution, employing strategies to create more inclusive datasets, robust evaluation frameworks for bias detection and correction, and mechanisms to minimize hallucinations, ensuring responsible and equitable outcomes.

## 8 CONCLUSION

This survey paper provides a thorough exploration of the integration of LLMs with 3D data. Systematically reviewing methodologies, applications, and emergent abilities of LLMs in processing, understanding, and generating 3D data, the survey underlines the transformative potential of LLMs across a spectrum of 3D tasks. From enhancing spatial comprehension and interaction within 3D environments to driving forward the capabilities of embodied AI systems, LLMs emerge as pivotal in advancing the field.

Key findings include the identification of LLMs’ unique advantages such as zero-shot learning, advanced reasoning, and extensive world knowledge, which are instrumental in bridging the gap between textual information and spatial interpretation. The paper showcases the wide array of tasks where LLMs’ integration with 3D data has been successfully demonstrated. The exploration of other 3D vision-language methods alongside LLMs reveals a rich landscape of research aiming to deepen our understanding of the 3D world.

Furthermore, the survey highlights significant challenges such as data representation, model scalability, and computational efficiency, suggesting that overcoming these hurdles is crucial for the full realization of LLMs’ potential in 3D applications. In conclusion, this survey not only offers a comprehensive overview of the current state of 3D tasks using LLMs but also sets the stage for future research directions. It calls for a collaborative effort to explore and expand the capabilities of LLMs in understanding and interacting with the complex 3D world, paving the way for further advancements in the area of spatial intelligence.

## REFERENCES

- [1] L. Chen et al. Driving with llms: Fusing object-level vector modality for explainable autonomous driving. *arXiv preprint arXiv:2310.01957*, 2023.

- [2] H. Sha et al. Languagempc: Large language models as decision makers for autonomous driving. *arXiv preprint arXiv:2310.03026*, 2023.
- [3] D. Fu et al. Drive like a human: Rethinking autonomous driving with large language models. In *WACV*, pp. 910–919, 2024.
- [4] Z. Xu et al. Drivepvt4: Interpretable end-to-end autonomous driving via large language model. *arXiv preprint arXiv:2310.01412*, 2023.
- [5] X. Ma et al. Both style and fog matter: Cumulative domain adaptation for semantic foggy scene understanding. In *CVPR*, pp. 18922–18931, 2022.
- [6] R. T. Azuma. A survey of augmented reality. *Presence: teleoperators & virtual environments*, 6(4):355–385, 1997.
- [7] J. Carmigniani and B. Furht. Augmented reality: an overview. *Handbook of augmented reality*, pp. 3–46, 2011.
- [8] A. B. Craig. *Understanding augmented reality: Concepts and applications*. Newnes, 2013.
- [9] S. Feiner et al. A touring machine: Prototyping 3d mobile augmented reality systems for exploring the urban environment. *Personal Technologies*, 1:208–217, 1997.
- [10] A. Brohan et al. Rt-2: Vision-language-action models transfer web knowledge to robotic control. In *arXiv preprint arXiv:2307.15818*, 2023.
- [11] D. Zheng et al. Towards learning a generalist model for embodied navigation. *arXiv preprint arXiv:2312.02010*, 2023.
- [12] C. H. Song et al. Llm-planner: Few-shot grounded planning for embodied agents with large language models. In *ICCV*, pp. 2998–3009, 2023.
- [13] W. Huang et al. Voxposer: Composable 3d value maps for robotic manipulation with language models. *arXiv preprint arXiv:2307.05973*, 2023.
- [14] R. Mirjalili et al. Lan-grasp: Using large language models for semantic object grasping. *arXiv preprint arXiv:2310.05239*, 2023.
- [15] X. Li et al. Maniplm: Embodied multimodal large language model for object-centric robotic manipulation. *arXiv preprint arXiv:2312.16217*, 2023.
- [16] Z. Yuan et al. Visual programming for zero-shot open-vocabulary 3d visual grounding. *arXiv preprint arXiv:2311.15383*, 2023.
- [17] S. Zhang et al. Agent3d-zero: An agent for zero-shot 3d understanding, 2024.
- [18] K. M. Jatavallabhula et al. Conceptfusion: Open-set multimodal 3d mapping. *arXiv preprint arXiv:2302.07241*, 2023.
- [19] S. Chen et al. Ll3da: Visual interactive instruction tuning for omni-3d understanding, reasoning, and planning. *arXiv preprint arXiv:2311.18651*, 2023.
- [20] Z. Guo et al. Viewrefer: Grasp the multi-view knowledge for 3d visual grounding with gpt and prototype guidance. *arXiv preprint arXiv:2303.16894*, 2023.
- [21] J. Yang et al. Llm-grounder: Open-vocabulary 3d visual grounding with large language model as an agent. *arXiv preprint arXiv:2309.12311*, 2023.
- [22] A. Abdelreheem et al. Zero-shot 3d shape correspondence. In *SIGGRAPH Asia 2023 Conference Papers*, pp. 1–11, 2023.
- [23] J. Fang et al. Transcribe3d: Grounding llms using transcribed information for 3d referential reasoning with self-corrected finetuning. In *2nd Workshop on Language and Robot Learning: Language as Grounding*, 2023.
- [24] Y. Hong et al. Multiply: A multisensory object-centric embodied large language model in 3d world. *arXiv preprint arXiv:2401.08577*, 2024.
- [25] X. Zhou et al. Gala3d: Towards text-to-3d complex scene generation via layout-guided generative gaussian splatting. *arXiv preprint arXiv:2402.07207*, 2024.
- [26] C. Sun et al. 3d-gpt: Procedural 3d modeling with large language models. *arXiv preprint arXiv:2310.12945*, 2023.
- [27] D. Z. Chen et al. D3net: A unified speaker-listener architecture for 3d dense captioning and visual grounding. In *ECCV*, pp. 487–505. Springer, 2022.
- [28] X. Li et al. Uni3d: Unified model for 3d and language understanding. *arXiv:2310.09478*, 2023.
- [29] S. Peng et al. Openscene: 3d scene understanding with open vocabularies. In *CVPR*, 2023.
- [30] J. Kerr et al. Lrf: Language embedded radiance fields. In *ICCV*, 2023.
- [31] B. Poole et al. Dreamfusion: Text-to-3d using 2d diffusion. *arXiv preprint arXiv:2209.14988*, 2022.
- [32] N. M. Khalid et al. Clip-mesh: Generating textured meshes from text using pretrained image-text models. *arXiv preprint arXiv:2203.13333*, 2022.
- [33] C. R. Qi et al. Pointnet: Deep learning on point sets for 3d classification and segmentation. In *CVPR*, 2017.
- [34] C. R. Qi et al. Pointnet++: Deep hierarchical feature learning on point sets in a metric space. *NeurIPS*, 30, 2017.
- [35] R. Roveri et al. PointProNets: Consolidation of Point Clouds with Convolutional Neural Networks. In *CGF*, 2018.
- [36] X. Liu et al. Flownet3d: Learning scene flow in 3d point clouds. In *CVPR*, 2019.
- [37] Z. Wang et al. Flownet3d++: Geometric losses for deep scene flow estimation. In *WACV*, 2020.
- [38] W. Yifan et al. Differentiable surface splatting for point-based geometry processing. In *ACM TOG*, 2019.
- [39] O. Wiles et al. SynSin: End-to-end View Synthesis from a Single Image. In *CVPR*, 2020.
- [40] C.-H. Lin et al. Learning Efficient Point Cloud Generation for Dense 3D Object Reconstruction. In *AAAI*, 2018.
- [41] L. Li et al. End-to-End Learning Local Multi-view Descriptors for 3D Point Clouds. In *CVPR*, 2020.
- [42] E. Insafutdinov and A. Dosovitskiy. Unsupervised Learning of Shape and Pose with Differentiable Point Clouds. In *NeurIPS*, 2018.
- [43] B. Fei et al. Comprehensive review of deep learning-based 3d point cloud completion processing and analysis. *IEEE Transactions on Intelligent Transportation Systems*, 2022.
- [44] X. Yan et al. Perspective transformer nets: Learning single-view 3d object reconstruction without 3d supervision. In *NeurIPS*, 2016.
- [45] A. Dai et al. Shape completion using 3d-encoder-predictor cnns and shape synthesis. In *CVPR*, pp. 5868–5877, 2017.
- [46] A. Dai and M. Nießner. 3dmv: Joint 3d-multi-view prediction for 3d semantic scene segmentation. In *ECCV*, pp. 452–468, 2018.
- [47] S. Tulsiani et al. Multi-view supervision for single-view reconstruction via differentiable ray consistency. In *IEEE TPAMI*, 2019.
- [48] P. Henzler et al. Escaping Plato’s Cave: 3D Shape From Adversarial Rendering. In *ICCV*, 2019.
- [49] S. Lombardi et al. Neural volumes: Learning dynamic renderable volumes from images. In *ACM TOG*, 2019.
- [50] Y. Jiang et al. Sdfdiff: Differentiable rendering of signed distance fields for 3d shape optimization. In *CVPR*, 2020.
- [51] K. Schwarz et al. Voxgraf: Fast 3d-aware image synthesis with sparse voxel grids. *NeurIPS*, 2022.
- [52] Q. Xu et al. A survey of deep learning-based 3d shape generation. In *Computational Visual Media*, 2023.
- [53] D. Peng et al. A pde-based fast local level set method. *Journal of Computational Physics*, 1999.
- [54] S. Osher et al. Level set methods and dynamic implicit surfaces. *Applied Mechanics Reviews*, 2004.
- [55] V. A. Prisacariu and I. Reid. Shared shape spaces. In *ICCV*, 2011.
- [56] Q. Xu et al. Disn: Deep implicit surface network for high-quality single-view 3d reconstruction. *NeurIPS*, 2019.
- [57] Y. Jiang et al. Sdfdiff: Differentiable rendering of signed distance fields for 3d shape optimization. In *CVPR*, 2020.
- [58] B. Curless and M. Levoy. A volumetric method for building complex models from range images. In *The 23rd annual conference on Computer graphics and interactive techniques*, 1996.
- [59] R. A. Newcombe et al. Kinectfusion: Real-time dense surface mapping and tracking. In *ISMAR*, 2011.
- [60] M. Niessner et al. Real-time 3d reconstruction at scale using voxel hashing. *ACM TOG*, 2013.
- [61] A. Dai et al. Bundlefusion: Real-time globally consistent 3d reconstruction using on-the-fly surface reintegration. *ACM TOG*, 36(4):1, 2017.
- [62] A. Dai et al. Sg-nn: Sparse generative neural networks for self-supervised scene completion of rgb-d scans. In *CVPR*, pp. 849–858, 2020.
- [63] P. Mittal et al. Autosdf: Shape priors for 3d completion, reconstruction and generation. In *CVPR*, 2022.
- [64] H. Kato et al. Differentiable rendering: A survey. In *arXiv*, 2020.
- [65] H. Kato et al. Neural 3D Mesh Renderer. In *CVPR*, 2018.
- [66] K. Genova et al. Unsupervised Training for 3D Morphable Model Regression. In *CVPR*, 2018.
- [67] M. M. Loper and M. J. Black. OpenDR: An approximate differentiable renderer. In *ECCV*, 2014.
- [68] H. Kato and T. Harada. Learning view priors for single-view 3d reconstruction. In *CVPR*, 2019.
- [69] H. Rhodin et al. A Versatile Scene Model with Differentiable Visibility Applied to Generative Pose Estimation. In *ICCV*, 2015.
- [70] S. Liu et al. Soft Rasterizer: A Differentiable Renderer for Image-Based 3D Reasoning. In *ICCV*, 2019.
- [71] W. Chen et al. Learning to Predict 3D Objects with an Interpolationbased Differentiable Renderer. In *NeurIPS*, 2019.
- [72] Y. Xie et al. Neural fields in visual computing and beyond. In *CGF*, 2022.
- [73] A. Tewari et al. State of the art on neural rendering. In *CGF*, 2020.
- [74] L. Mescheder et al. Occupancy networks: Learning 3d reconstruction in function space. In *CVPR*, 2019.
- [75] S. Peng et al. Convolutional occupancy networks. In *ECCV*, 2020.
- [76] Z. Chen and H. Zhang. Learning implicit fields for generative shape modeling. In *CVPR*, 2019.
- [77] J. J. Park et al. DeepSDF: Learning continuous signed distance functions for shape representation. In *CVPR*, 2019.
- [78] V. Sitzmann et al. Scene representation networks: Continuous 3d-structure aware neural scene representations. In *NeurIPS*, 2019.
- [79] P. Wang et al. Neus: Learning neural implicit surfaces by volume rendering for multi-view reconstruction. *NeurIPS*, 2021.
- [80] Y. Wang et al. Neus2: Fast learning of neural implicit surfaces for multi-view reconstruction. In *ICCV*, 2023.
- [81] B. Mildenhall et al. NeRF Representing scenes as neural radiance fields for view synthesis. In *ECCV*, 2020.
- [82] R. Martin-Brualla et al. NeRF in the Wild: Neural Radiance Fields for Unconstrained Photo Collections. In *CVPR*, 2021.
- [83] K. Zhang et al. Nerf++: Analyzing and improving neural radiance fields. *arXiv:2010.07492*, 2020.
- [84] Z. Wang et al. NeRF—: Neural radiance fields without known camera parameters. *arXiv preprint arXiv:2102.07064*, 2021.
- [85] Z. Li et al. Neural scene flow fields for space-time view synthesis of dynamic scenes. In *CVPR*, 2021.
- [86] A. Pumarola et al. D-nerf: Neural radiance fields for dynamic scenes. In *CVPR*, 2021.
- [87] K. Schwarz et al. Graf: Generative radiance fields for 3d-aware image synthesis. In *NeurIPS*, 2020.
- [88] M. Niemeyer and A. Geiger. Giraffe: Representing scenes as compositional generative neural feature fields. In *CVPR*, 2021.
- [89] D. Rebaïn et al. Derf: Decomposed radiance fields. In *CVPR*, 2021.
- [90] K. Park et al. Deformable Neural Radiance Fields. *ICCV*, 2021.
- [91] W. Xian et al. Space-time neural irradiance fields for free-viewpoint video. In *CVPR*, 2021.
- [92] W. Bian et al. Nope-nerf: Optimising neural radiance field with no pose prior. In

- CVPR, 2023.
- [93] J.-W. Bian et al. Porf: Pose residual field for accurate neural surface reconstruction. *arXiv preprint arXiv:2310.07449*, 2023.
- [94] J. T. Barron et al. Mip-nerf 360: Unbounded anti-aliased neural radiance fields. In *CVPR*, 2022.
- [95] A. Vaswani et al. Attention is all you need. In *NeurIPS*, 2017.
- [96] M. Tancik et al. Fourier features let networks learn high frequency functions in low dimensional domains. In *NeurIPS*, 2020.
- [97] S.-F. Chng et al. Gaussian activated neural radiance fields for high fidelity reconstruction and pose estimation. In *ECCV*, 2022.
- [98] L. Liu et al. Neural sparse voxel fields. *NeurIPS*, 2020.
- [99] C. Sun et al. Direct voxel grid optimization: Super-fast convergence for radiance fields reconstruction. In *CVPR*, 2022.
- [100] A. Yu et al. Plenoxels: Radiance fields without neural networks. *CVPR*, 2022.
- [101] Z. Chen et al. Mobilenerf: Exploiting the polygon rasterization pipeline for efficient neural field rendering on mobile architectures. In *CVPR*, 2023.
- [102] T. Müller et al. Instant neural graphics primitives with a multiresolution hash encoding. *ACM TOG*, 2022.
- [103] B. Kerbl et al. 3d gaussian splatting for real-time radiance field rendering. *ACM Transactions on Graphics*, 2023.
- [104] C. Reiser et al. Merf: Memory-efficient radiance fields for real-time view synthesis in unbounded scenes. *SIGGRAPH*, 2023.
- [105] D. Duckworth et al. Smerf: Streamable memory efficient radiance fields for real-time large-scene exploration. *arXiv preprint arXiv:2312.07541*, 2023.
- [106] T. Lu et al. Scaffold-gs: Structured 3d gaussians for view-adaptive rendering. *CVPR*, 2024.
- [107] J. C. Lee et al. Compact 3d gaussian representation for radiance field. *CVPR*, 2024.
- [108] J. L. Schönberger and J.-M. Frahm. Structure-from-motion revisited. In *CVPR*, 2016.
- [109] C. Lassner and M. Zollhofer. Pulsar: Efficient sphere-based neural rendering. In *CVPR*, 2021.
- [110] J. L. Elman. Finding structure in time. *Cognitive science*, 1990.
- [111] S. Hochreiter and J. Schmidhuber. Long short-term memory. *Neural computation*, 1997.
- [112] J. Kaplan et al. Scaling laws for neural language models. *arXiv preprint arXiv:2001.08361*, 2020.
- [113] W. X. Zhao et al. A survey of large language models. *arXiv preprint arXiv:2303.18223*, 2023.
- [114] S. Minaee et al. Large language models: A survey. *arXiv preprint arXiv:2402.06196*, 2024.
- [115] J. Wei et al. Emergent abilities of large language models. *arXiv preprint arXiv:2206.07682*, 2022.
- [116] Q. Dong et al. A survey on in-context learning. *arXiv preprint arXiv:2301.00234*, 2023.
- [117] T. Lin et al. A survey of transformers. *AI open*, 2022.
- [118] M. Lewis et al. Bart: Denoising sequence-to-sequence pre-training for natural language generation, translation, and comprehension. *arXiv preprint arXiv:1910.13461*, 2019.
- [119] C. Raffel et al. Exploring the limits of transfer learning with a unified text-to-text transformer. In *JMLR*, 2020.
- [120] P. J. Liu et al. Generating wikipedia by summarizing long sequences. *arXiv preprint arXiv:1801.10198*, 2018.
- [121] A. Radford et al. Improving language understanding by generative pre-training. *OpenAI*, 2018.
- [122] T. Le Scao et al. Bloom: A 176b-parameter open-access multilingual language model. *ArXiv*, abs/2211.05100, 2022.
- [123] R. Sennrich et al. Neural machine translation of rare words with subword units. *arXiv preprint arXiv:1508.07909*, 2015.
- [124] M. Schuster and K. Nakajima. Japanese and korean voice search. In *International Conference on Acoustics, Speech and Signal Processing*, pp. 5149–5152, 2012.
- [125] T. Kudo and J. Richardson. Sentencepiece: A simple and language independent subword tokenizer and detokenizer for neural text processing. *arXiv preprint arXiv:1808.06226*, 2018.
- [126] Y. Kim et al. Structured attention networks. *arXiv preprint arXiv:1702.00887*, 2017.
- [127] T. Brown et al. Language models are few-shot learners. *NeurIPS*, 33:1877–1901, 2020.
- [128] J. Liu et al. What makes good in-context examples for gpt-3? *arXiv preprint arXiv:2101.06804*, 2021.
- [129] S. Min et al. Rethinking the role of demonstrations: What makes in-context learning work? *arXiv preprint arXiv:2202.12837*, 2022.
- [130] A. Radford et al. Language models are unsupervised multitask learners. *OpenAI blog*, 1(8):9, 2019.
- [131] J. Achiam et al. Gpt-4 technical report. *arXiv preprint arXiv:2303.08774*, 2023.
- [132] J. Wei et al. Chain-of-thought prompting elicits reasoning in large language models. *NeurIPS*, 35:24824–24837, 2022.
- [133] Z. Zhang et al. Automatic chain of thought prompting in large language models. In *ICLR*, 2023.
- [134] D. Hendrycks et al. Measuring mathematical problem solving with the math dataset. *NeurIPS*, 2021.
- [135] D. Saxton et al. Analysing mathematical reasoning abilities of neural models. *ICLR*, 2019.
- [136] A. Patel et al. Are NLP models really able to solve simple math word problems? In *Proceedings of the 2021 Conference of the North American Chapter of the Association for Computational Linguistics: Human Language Technologies*, 2021.
- [137] S.-y. Miao et al. A diverse corpus for evaluating and developing english math word problem solvers. In *Proceedings of the 58th Annual Meeting of the Association for Computational Linguistics*, pp. 975–984, 2020.
- [138] A. Wang et al. Glue: A multi-task benchmark and analysis platform for natural language understanding. *ICLR*, 2019.
- [139] C. Raffel et al. Exploring the limits of transfer learning with a unified text-to-text transformer. *Journal of Machine Learning Research (JMLR)*, 2020.
- [140] H. Touvron et al. Llama: Open and efficient foundation language models. *arXiv preprint arXiv:2302.13971*, 2023.
- [141] H. Touvron et al. Llama 2: Open foundation and fine-tuned chat models. *arXiv preprint arXiv:2307.09288*, 2023.
- [142] J. Devlin et al. Bert: Pre-training of deep bidirectional transformers for language understanding. *arXiv preprint arXiv:1810.04805*, 2018.
- [143] M. AI. Introducing meta llama 3: The most capable openly available llm to date. <https://ai.meta.com/blog/meta-llama-3/>, April 2024.
- [144] L. Ouyang et al. Training language models to follow instructions with human feedback. *NeurIPS*, 2022.
- [145] R. Taori et al. Stanford alpaca: An instruction-following llama model. [https://github.com/tatsu-lab/stanford\\_alpaca](https://github.com/tatsu-lab/stanford_alpaca), 2023.
- [146] H. W. Chung et al. Scaling instruction-finetuned language models. *arXiv preprint arXiv:2210.11416*, 2022.
- [147] S. Mangrulkar et al. Pefit: State-of-the-art parameter-efficient fine-tuning methods. <https://github.com/huggingface/peft>, 2022.
- [148] E. J. Hu et al. Lora: Low-rank adaptation of large language models. *arXiv preprint arXiv:2106.09685*, 2021.
- [149] T. Dettmers et al. Qlora: Efficient finetuning of quantized llms. *NeurIPS*, 36, 2024.
- [150] L. Zhang et al. Lora-fa: Memory-efficient low-rank adaptation for large language models fine-tuning. *arXiv preprint arXiv:2308.03303*, 2023.
- [151] J. Yosinski et al. How transferable are features in deep neural networks? *NeurIPS*, 2014.
- [152] J. Howard and S. Ruder. Universal language model fine-tuning for text classification. In *Proceedings of the 56th Annual Meeting of the Association for Computational Linguistics (Volume 1: Long Papers)*, 2018.
- [153] Y. Hong et al. 3d-llm: Injecting the 3d world into large language models. *NeurIPS*, 2023.
- [154] B. Lester et al. The power of scale for parameter-efficient prompt tuning. In *Proceedings of the 2021 Conference on Empirical Methods in Natural Language Processing*, pp. 3045–3059, 2021.
- [155] P. Liu et al. Pre-train, prompt, and predict: A systematic survey of prompting methods in natural language processing. *ACM Computing Surveys*, 55(9):1–35, 2023.
- [156] J. Gu et al. A systematic survey of prompt engineering on vision-language foundation models. *arXiv preprint arXiv:2307.12980*, 2023.
- [157] T. Kojima et al. Large language models are zero-shot reasoners. In *NeurIPS*, 2022.
- [158] Y. Wang et al. Super-naturalinstructions: Generalization via declarative instructions on 1600+ nlp tasks. *arXiv preprint arXiv:2204.07705*, 2022.
- [159] V. Sanh et al. Multitask prompted training enables zero-shot task generalization. In *ICLR*, 2022.
- [160] T. Shin et al. Autoprompt: Eliciting knowledge from language models with automatically generated prompts. *arXiv preprint arXiv:2010.15980*, 2020.
- [161] Z. Jiang et al. How can we know what language models know? *Transactions of the Association for Computational Linguistics*, 2020.
- [162] A. Prasad et al. Grips: Gradient-free, edit-based instruction search for prompting large language models. *arXiv preprint arXiv:2203.07281*, 2022.
- [163] Y. Wen et al. Hard prompts made easy: Gradient-based discrete optimization for prompt tuning and discovery. *NeurIPS*, 2024.
- [164] T. Vu et al. Spot: Better frozen model adaptation through soft prompt transfer. *arXiv preprint arXiv:2110.07904*, 2021.
- [165] X. L. Li and P. Liang. Prefix-tuning: Optimizing continuous prompts for generation. *arXiv preprint arXiv:2101.00190*, 2021.
- [166] Y. Gu et al. Ppt: Pre-trained prompt tuning for few-shot learning. In *ACL*, pp. 8410–8423, 2022.
- [167] Y. Su et al. On transferability of prompt tuning for natural language processing. *arXiv preprint arXiv:2111.06719*, 2021.
- [168] H. Wu and X. Shi. Adversarial soft prompt tuning for cross-domain sentiment analysis. *Proceedings of the 60th Annual Meeting of the Association for Computational Linguistics*, 2022.
- [169] X. Li et al. Sd4match: Learning to prompt stable diffusion model for semantic matching. *arXiv preprint arXiv:2310.17569*, 2023.
- [170] J. Wu et al. Infoprompt: Information-theoretic soft prompt tuning for natural language understanding. *NeurIPS*, 2024.
- [171] Z. Wang et al. Chat-3d: Data-efficiently tuning large language model for universal dialogue of 3d scenes, 2023.
- [172] H. Huang et al. Chat-3d v2: Bridging 3d scene and large language models with object identifiers. *arXiv preprint arXiv:2312.08168*, 2023.
- [173] J. Pfeiffer et al. Adapterhub: A framework for adapting transformers. *arXiv preprint arXiv:2007.07779*, 2020.
- [174] A. Radford et al. Learning transferable visual models from natural language supervision. In *ICML*, pp. 8748–8763. PMLR, 2021.
- [175] C. Jia et al. Scaling up visual and vision-language representation learning with noisy text supervision. In *ICML*, 2021.
- [176] J. Yang et al. Unified contrastive learning in image-text-label space. In *CVPR*, 2022.
- [177] W. Kim et al. Vilt: Vision-and-language transformer without convolution or region supervision. In *ICML*, 2021.
- [178] Y. Li et al. Supervision exists everywhere: A data efficient contrastive language-image pre-training paradigm. In *ICLR*, 2022.
- [179] A. Singh et al. Flava: A foundational language and vision alignment model. In

- CVPR, pp. 15638–15650, 2022.
- [180] X. Gu et al. Open-vocabulary detection via vision and language knowledge distillation. *arXiv preprint arXiv:2104.13921*, 2021.
- [181] H. Rasheed et al. Bridging the gap between object and image-level representations for open-vocabulary detection. In *NeurIPS*, 2022.
- [182] M. Minderer et al. Simple open-vocabulary object detection with vision transformers. In *ECCV*, 2022.
- [183] Y. Zhong et al. Regionclip: Region-based language-image pretraining. In *CVPR*, 2022.
- [184] T. Lüddecke and A. Ecker. Image segmentation using text and image prompts. In *CVPR*, 2022.
- [185] F. Liang et al. Open-vocabulary semantic segmentation with mask-adapted clip. In *CVPR*, 2023.
- [186] J. Ding et al. Decoupling zero-shot semantic segmentation. In *CVPR*, pp. 11583–11592, 2022.
- [187] B. Li et al. Language-driven semantic segmentation. In *ICLR*, 2022.
- [188] G. Ghiasi et al. Scaling open-vocabulary image segmentation with image-level labels. In *ECCV*, 2022.
- [189] G. Kim et al. Ocr-free document understanding transformer. In *ECCV*, 2022.
- [190] Y. Xu et al. Layoutlm: Pre-training of text and layout for document image understanding. In *Proceedings of the 26th ACM SIGKDD International Conference on Knowledge Discovery & Data Mining*, 2020.
- [191] B. Ni et al. Expanding language-image pretrained models for general video recognition. In *ECCV*, 2022.
- [192] Z. Wang et al. SimVLM: Simple visual language model pretraining with weak supervision. In *ICLR*, 2022.
- [193] J. Li et al. Blip: Bootstrapping language-image pre-training for unified vision-language understanding and generation. In *ICML*, pp. 12888–12900. PMLR, 2022.
- [194] P. Wang et al. Ofa: Unifying architectures, tasks, and modalities through a simple sequence-to-sequence learning framework. In *ICML*, pp. 23318–23340. PMLR, 2022.
- [195] J. Li et al. Blip-2: Bootstrapping language-image pre-training with frozen image encoders and large language models. *arXiv preprint arXiv:2301.12597*, 2023.
- [196] J.-B. Alayrac et al. Flamingo: a visual language model for few-shot learning. *NeurIPS*, 35:23716–23736, 2022.
- [197] H. Liu et al. Visual instruction tuning. In *NeurIPS*, 2024.
- [198] J. Ho et al. Denoising diffusion probabilistic models. In *NeurIPS*, 2020.
- [199] Y. Song et al. Score-based generative modeling through stochastic differential equations. In *ICLR*, 2021.
- [200] J. Ho and T. Salimans. Classifier-free diffusion guidance. *arXiv preprint arXiv:2207.12598*, 2022.
- [201] R. Rombach et al. High-resolution image synthesis with latent diffusion models. In *CVPR*, 2022.
- [202] J. Ho et al. Imagen video: High definition video generation with diffusion models. *arXiv preprint arXiv:2210.02303*, 2022.
- [203] U. Singer et al. Text-to-4d dynamic scene generation. *arXiv preprint arXiv:2301.11280*, 2023.
- [204] A. Hertz et al. Prompt-to-prompt image editing with cross attention control. *arXiv preprint arXiv:2208.01626*, 2022.
- [205] T. Brooks et al. Instructpix2pix: Learning to follow image editing instructions. In *CVPR*, 2023.
- [206] R. Mokady et al. Null-text inversion for editing real images using guided diffusion models. In *CVPR*, 2023.
- [207] J. Wu et al. Gaussctrl: Multi-view consistent text-driven 3d gaussian splatting editing, 2024.
- [208] M. Caron et al. Emerging properties in self-supervised vision transformers. In *ICCV*, 2021.
- [209] J. Zhou et al. ibot: Image bert pre-training with online tokenizer. In *ICLR*, 2022.
- [210] M. Quab et al. Dinov2: Learning robust visual features without supervision. *arXiv preprint arXiv:2304.07193*, 2023.
- [211] A. Kirillov et al. Segment anything. *arXiv preprint arXiv:2304.02643*, 2023.
- [212] H. Zhang et al. Dino: Detr with improved denoising anchor boxes for end-to-end object detection. *arXiv preprint arXiv:2203.03605*, 2022.
- [213] N. Carion et al. End-to-end object detection with transformers. In *ECCV*, 2020.
- [214] S. Liu et al. Grounding dino: Marrying dino with grounded pre-training for open-set object detection. *arXiv preprint arXiv:2303.05499*, 2023.
- [215] L. Tang et al. Emergent correspondence from image diffusion. *NeurIPS*, 2024.
- [216] J. Tian et al. Diffuse, attend, and segment: Unsupervised zero-shot segmentation using stable diffusion. *arXiv preprint arXiv:2308.12469*, 2023.
- [217] Z. Chen et al. Scan2cap: Context-aware dense captioning in rgb-d scans. In *CVPR*, pp. 3193–3203, 2021.
- [218] D. Z. Chen et al. Scanrefer: 3d object localization in rgb-d scans using natural language. *ECCV*, 2020.
- [219] A. Celikyilmaz et al. Evaluation of text generation: A survey. *arXiv preprint arXiv:2006.14799*, 2020.
- [220] K. Papineni et al. Bleu: a method for automatic evaluation of machine translation. In *Proceedings of the 40th annual meeting of the Association for Computational Linguistics*, pp. 311–318, 2002.
- [221] C.-Y. Lin. Rouge: A package for automatic evaluation of summaries. In *Text summarization branches out*, pp. 74–81, 2004.
- [222] S. Banerjee and A. Lavie. Meteor: An automatic metric for mt evaluation with improved correlation with human judgments. In *Proceedings of the acl workshop on intrinsic and extrinsic evaluation measures for machine translation and/or summarization*, pp. 65–72, 2005.
- [223] R. Vedantam et al. Cider: Consensus-based image description evaluation. In *CVPR*, pp. 4566–4575, 2015.
- [224] N. Reimers and I. Gurevych. Sentence-bert: Sentence embeddings using siamese bert-networks. *arXiv preprint arXiv:1908.10084*, 2019.
- [225] T. Zhang et al. Bertscore: Evaluating text generation with bert. *arXiv preprint arXiv:1904.09675*, 2019.
- [226] S. Chen et al. End-to-end 3d dense captioning with vote2cap-detr. In *CVPR*, pp. 11124–11133, 2023.
- [227] Z. Chen et al. Unit3d: A unified transformer for 3d dense captioning and visual grounding. In *ICCV*, pp. 18109–18119, 2023.
- [228] P. Achlioptas et al. Referit3d: Neural listeners for fine-grained 3d object identification in real-world scenes. In *ECCV*, pp. 422–440. Springer, 2020.
- [229] Z. Lu et al. Scanneru: Interactive 3d visual grounding based on embodied reference understanding. *arXiv preprint arXiv:2303.13186*, 2023.
- [230] Y. Zhang et al. Multi3drefer: Grounding text description to multiple 3d objects. In *ICCV*, pp. 15225–15236, 2023.
- [231] W. Huang et al. Dense object grounding in 3d scenes. In *Proceedings of the 31st ACM International Conference on Multimedia*, pp. 5017–5026, 2023.
- [232] P.-H. Huang et al. Text-guided graph neural networks for referring 3d instance segmentation. In *AAAI*, volume 35, pp. 1610–1618, 2021.
- [233] X. Ma et al. Sqa3d: Situated question answering in 3d scenes. *arXiv preprint arXiv:2210.07474*, 2022.
- [234] D. Azuma et al. Scanqa: 3d question answering for spatial scene understanding. In *CVPR*, 2022.
- [235] T. Qian et al. Nuscenescs-qa: A multi-modal visual question answering benchmark for autonomous driving scenario. *arXiv preprint arXiv:2305.14836*, 2023.
- [236] Y. Hong et al. 3d concept learning and reasoning from multi-view images. In *CVPR*, pp. 9202–9212, 2023.
- [237] P. Anderson et al. Spice: Semantic propositional image caption evaluation. In *ECCV*, pp. 382–398. Springer, 2016.
- [238] P. Anderson et al. On evaluation of embodied navigation agents. *arXiv preprint arXiv:1807.06757*, 2018.
- [239] P. Anderson et al. Vision-and-language navigation: Interpreting visually-grounded navigation instructions in real environments. In *CVPR*, pp. 3674–3683, 2018.
- [240] G. Itharco et al. General evaluation for instruction conditioned navigation using dynamic time warping. *arXiv preprint arXiv:1907.05446*, 2019.
- [241] J. Gu et al. Vision-and-language navigation: A survey of tasks, methods, and future directions. *arXiv preprint arXiv:2203.12667*, 2022.
- [242] M. Shridhar et al. Cliport: What and where pathways for robotic manipulation. In *Conference on robot learning*, pp. 894–906. PMLR, 2022.
- [243] H.-H. Lee et al. Text-to-3d shape generation. *arXiv preprint arXiv:2403.13289*, 2024.
- [244] L. Xue et al. Ulip: Learning a unified representation of language, images, and point clouds for 3d understanding. In *CVPR*, pp. 1179–1189, 2023.
- [245] T. Wu et al. Gpt-4v (ision) is a human-aligned evaluator for text-to-3d generation. *arXiv preprint arXiv:2401.04092*, 2024.
- [246] I. Armeni et al. 3d semantic parsing of large-scale indoor spaces. In *CVPR*, pp. 1534–1543, 2016.
- [247] S. Sengupta et al. Urban 3d semantic modelling using stereo vision. In *ICRA*, pp. 580–585. IEEE, 2013.
- [248] J. McCormac et al. Semanticfusion: Dense 3d semantic mapping with convolutional neural networks. In *ICRA*, pp. 4628–4635. IEEE, 2017.
- [249] J. Huang et al. Generative 3d part assembly via dynamic graph learning. In *NeurIPS*, 2020.
- [250] J. Cheng et al. Score-pa: Score-based 3d part assembly. *British Machine Vision Conference*, 2023.
- [251] L. Jiang et al. Pointgroup: Dual-set point grouping for 3d instance segmentation. In *CVPR*, pp. 4867–4876, 2020.
- [252] J. Hou et al. 3d-sis: 3d semantic instance segmentation of rgb-d scans. In *CVPR*, pp. 4421–4430, 2019.
- [253] W. Wang et al. Sgpn: Similarity group proposal network for 3d point cloud instance segmentation. In *CVPR*, pp. 2569–2578, 2018.
- [254] L. Han et al. Occuseg: Occupancy-aware 3d instance segmentation. In *CVPR*, pp. 2940–2949, 2020.
- [255] X. Song et al. Apollocar3d: A large 3d car instance understanding benchmark for autonomous driving. In *CVPR*, pp. 5452–5462, 2019.
- [256] G. Zhan et al. Amodal ground truth and completion in the wild. In *CVPR*, 2024.
- [257] G. Zhan et al. What does stable diffusion know about the 3d scene? In *arXiv:2310.06836*, 2023.
- [258] M. Feng et al. Exploring hierarchical spatial layout cues for 3d point cloud based scene graph prediction. *IEEE Transactions on Multimedia*, 2023.
- [259] C. Zhang et al. Holistic 3d scene understanding from a single image with implicit representation. In *CVPR*, pp. 8833–8842, 2021.
- [260] C. Zhang et al. Deeppanocontext: Panoramic 3d scene understanding with holistic scene context graph and relation-based optimization. In *ICCV*, pp. 12632–12641, 2021.
- [261] G. Zhan et al. A tri-layer plugin to improve occluded detection. *British Machine Vision Conference*, 2022.
- [262] A. Delitzas et al. SceneFun3D: Fine-grained functionality and affordance understanding in 3d scenes. In *CVPR*, 2024.
- [263] K. Cheng et al. Learning environment-aware affordance for 3d articulated object manipulation under occlusions. In *NeurIPS*, 2023.
- [264] Y. Qiu et al. 3d-aware scene change captioning from multiview images. *IEEE Robotics and Automation Letters*, 2020.
- [265] S. Looper et al. 3d vsq: Long-term semantic scene change prediction through 3d variable scene graphs. In *ICRA*, pp. 8179–8186. IEEE, 2023.
- [266] R. Fu et al. Scene-llm: Extending language model for 3d visual understanding and reasoning, 2024.
- [267] R. Xu et al. Pointllm: Empowering large language models to understand point clouds. *arXiv preprint arXiv:2308.16911*, 2023.

- [268] Z. Qi et al. Gpt4point: A unified framework for point-language understanding and generation. *arXiv preprint arXiv:2312.02980*, 2023.
- [269] Z. Li et al. 3dmit: 3d multi-modal instruction tuning for scene understanding. *arXiv preprint arXiv:2401.03201*, 2024.
- [270] J. Huang et al. An embodied generalist agent in 3d world. In *ICML*, 2024.
- [271] S. Yang et al. Lidar-llm: Exploring the potential of large language models for 3d lidar understanding. *arXiv preprint arXiv:2312.14074*, 2023.
- [272] Z. Guo et al. Point-bind & point-llm: Aligning point cloud with multi-modality for 3d understanding, generation, and instruction following. *arXiv preprint arXiv:2309.00615*, 2023.
- [273] D. Liu et al. 3daxiesprompts: Unleashing the 3d spatial task capabilities of gpt-4v. *arXiv preprint arXiv:2312.09738*, 2023.
- [274] W. Chen et al. Leveraging large language models for robot 3d scene understanding. *arXiv preprint arXiv:2209.05629*, 2022.
- [275] K. Rana et al. Sayplan: Grounding large language models using 3d scene graphs for scalable task planning. *arXiv preprint arXiv:2307.06135*, 2023.
- [276] H. Zhen et al. 3d-vla: A 3d vision-language-action generative world model. *arXiv preprint arXiv:2403.09631*, 2024.
- [277] Z. Xiao et al. Unified human-scene interaction via prompted chain-of-contacts. *arXiv preprint arXiv:2309.07918*, 2023.
- [278] X. L. Li et al. A systematic investigation of commonsense knowledge in large language models. In Y. Goldberg et al., editors, *Proceedings of the 2022 Conference on Empirical Methods in Natural Language Processing*, pp. 11838–11855, Abu Dhabi, United Arab Emirates, December 2022. Association for Computational Linguistics.
- [279] H. Wang et al. Beyond first impressions: Integrating joint multi-modal cues for comprehensive 3d representation. In *Proceedings of the 31st ACM International Conference on Multimedia*, pp. 3403–3414, 2023.
- [280] C. Nash et al. Polygen: An autoregressive generative model of 3d meshes. In *ICML*, pp. 7220–7229. PMLR, 2020.
- [281] F. De La Torre et al. Llmr: Real-time prompting of interactive worlds using large language models. *arXiv preprint arXiv:2309.12276*, 2023.
- [282] Y. Siddiqui et al. Meshgpt: Generating triangle meshes with decoder-only transformers. *arXiv preprint arXiv:2311.15475*, 2023.
- [283] F. Yin et al. Shapegpt: 3d shape generation with a unified multi-modal language model. *arXiv preprint arXiv:2311.17618*, 2023.
- [284] Y. Yang et al. Holodeck: Language guided generation of 3d embodied ai environments. In *CVPR*, volume 30, pp. 20–25. IEEE/CVF, 2024.
- [285] A. Chang et al. Matterport3d: Learning from rgb-d data in indoor environments. *International Conference on 3D Vision (3DV)*, 2017.
- [286] Chatgpt. <https://openai.com/blog/chatgpt>. Accessed: 2023-07-22.
- [287] D. He et al. Transrefer3d: Entity-and-relation aware transformer for fine-grained 3d visual grounding. In *Proceedings of the 29th ACM International Conference on Multimedia*, pp. 2344–2352, 2021.
- [288] X. Yu et al. Point-bert: Pre-training 3d point cloud transformers with masked point modeling. In *CVPR*, pp. 19313–19322, 2022.
- [289] J. Zhou et al. Uni3d: Exploring unified 3d representation at scale. In *ICLR*, 2024.
- [290] Q. Gu et al. Conceptgraphs: Open-vocabulary 3d scene graphs for perception and planning. *arXiv preprint arXiv:2309.16650*, 2023.
- [291] B. Cheng et al. Per-pixel classification is not all you need for semantic segmentation. In *NeurIPS*, 2021.
- [292] Y. Zhou and O. Tuzel. Voxynet: End-to-end learning for point cloud based 3d object detection. In *CVPR*, pp. 4490–4499, 2018.
- [293] M. Deitke et al. Objaverse: A universe of annotated 3d objects. In *CVPR*, pp. 13142–13153, 2023.
- [294] Z. Zhu et al. 3d-vista: Pre-trained transformer for 3d vision and text alignment. In *ICCV*, pp. 2911–2921, 2023.
- [295] J. Wald et al. Rio: 3d object instance re-localization in changing indoor environments. In *ICCV*, pp. 7658–7667, 2019.
- [296] A. X. Chang et al. Shapenet: An information-rich 3d model repository. *arXiv preprint arXiv:1512.03012*, 2015.
- [297] M. A. Uy et al. Revisiting point cloud classification: A new benchmark dataset and classification model on real-world data. In *ICCV*, 2019.
- [298] S. Zhang et al. Instruction tuning for large language models: A survey. *arXiv preprint arXiv:2308.10792*, 2023.
- [299] R. Beaumont. Clip retrieval: Easily compute clip embeddings and build a clip retrieval system with them, 2022.
- [300] A. Guzhov et al. Audioclip: Extending clip to image, text and audio. In *ICASSP 2022-2022 IEEE International Conference on Acoustics, Speech and Signal Processing (ICASSP)*, pp. 976–980, 2022.
- [301] N. Mu et al. Slip: Self-supervision meets language-image pre-training. In *ECCV*, pp. 529–544, 2022.
- [302] R. Girdhar et al. Imagebind: One embedding space to bind them all. In *CVPR*, pp. 15180–15190, 2023.
- [303] Z. Hu et al. SceneCraft: An LLM agent for synthesizing 3D scene as Blender code. In *ICLR 2024 Workshop on Large Language Model (LLM) Agents*, 2024.
- [304] J. Zhang et al. Clip-fo3d: Learning free open-world 3d scene representations from 2d dense clip. In *ICCV*, pp. 2048–2059, 2023.
- [305] H. Ha and S. Song. Semantic Abstraction: Open-world 3D scene understanding from 2D vision-language models. In *CoRL*, 2022.
- [306] K. Yamazaki et al. Open-fusion: Real-time open-vocabulary 3d mapping and queryable scene representation. *arXiv preprint arXiv:2310.03923*, 2023.
- [307] X. Zou et al. Segment everything everywhere all at once. *NeurIPS*, 36, 2024.
- [308] R. Ding et al. Pla: Language-driven open-vocabulary 3d scene understanding. In *CVPR*, 2023.
- [309] J. Yang et al. Regionplc: Regional point-language contrastive learning for open-world 3d scene understanding. *arXiv preprint arXiv:2304.00962*, 2023.
- [310] S. Lu et al. Ovir-3d: Open-vocabulary 3d instance retrieval without training on 3d data. In *Conference on Robot Learning*, pp. 1610–1620. PMLR, 2023.
- [311] Y. Cao et al. Coda: Collaborative novel box discovery and cross-modal alignment for open-vocabulary 3d object detection. *NeurIPS*, 36, 2023.
- [312] A. Takmaz et al. OpenMask3D: Open-Vocabulary 3D Instance Segmentation. In *NeurIPS*, 2023.
- [313] P. D. Nguyen et al. Open3dis: Open-vocabulary 3d instance segmentation with 2d mask guidance. *arXiv preprint arXiv:2312.10671*, 2023.
- [314] Z. Huang et al. Openins3d: Snap and lookup for 3d open-vocabulary instance segmentation. *arXiv preprint*, 2023.
- [315] D. Rozenberszki et al. Language-grounded indoor 3d semantic segmentation in the wild. In *ECCV*, pp. 125–141. Springer, 2022.
- [316] S. Kobayashi et al. Decomposing nerf for editing via feature field distillation. *NeurIPS*, 35:23311–23330, 2022.
- [317] N. Tsagkas et al. VI-fields: Towards language-grounded neural implicit spatial representations. *arXiv preprint arXiv:2305.12427*, 2023.
- [318] K. Liu et al. Weakly supervised 3d open-vocabulary segmentation. *NeurIPS*, 36, 2024.
- [319] M. Qin et al. Langsplat: 3d language gaussian splatting. *arXiv preprint arXiv:2312.16084*, 2023.
- [320] Y. Bhalgat et al. N2f2: Hierarchical scene understanding with nested neural feature fields, 2024.
- [321] R. Rombach et al. High-resolution image synthesis with latent diffusion models. In *CVPR*, pp. 10684–10695, 2022.
- [322] C. Saharia et al. Photorealistic text-to-image diffusion models with deep language understanding. *NeurIPS*, 35:36479–36494, 2022.
- [323] A. Jain et al. Zero-shot text-guided object generation with dream fields. In *CVPR*, pp. 867–876, 2022.
- [324] A. Sanghi et al. Clip-forge: Towards zero-shot text-to-shape generation. In *CVPR*, pp. 18603–18613, 2022.
- [325] O. Michel et al. Text2mesh: Text-driven neural stylization for meshes. In *CVPR*, pp. 13492–13502, 2022.
- [326] C.-H. Lin et al. Magic3d: High-resolution text-to-3d content creation. *arXiv preprint arXiv:2211.10440*, 2022.
- [327] R. Chen et al. Fantasia3d: Disentangling geometry and appearance for high-quality text-to-3d content creation. In *ICCV*, pp. 22246–22256, 2023.
- [328] T. Shen et al. Deep marching tetrahedra: a hybrid representation for high-resolution 3d shape synthesis. In *NeurIPS*, 2021.
- [329] Z. Wang et al. Prolificdreamer: High-fidelity and diverse text-to-3d generation with variational score distillation. *NeurIPS*, 36, 2024.
- [330] J. Xu et al. Dream3d: Zero-shot text-to-3d synthesis using 3d shape prior and text-to-image diffusion models. In *CVPR*, pp. 20908–20918, 2023.
- [331] Y. Shi et al. Mvdream: Multi-view diffusion for 3d generation. *arXiv preprint arXiv:2308.16512*, 2023.
- [332] J. Zhang et al. Text2nerf: Text-driven 3d scene generation with neural radiance fields. *IEEE Transactions on Visualization and Computer Graphics*, 2024.
- [333] E. Richardson et al. Texture: Text-guided texturing of 3d shapes. In *ACM SIGGRAPH 2023 Conference Proceedings*, pp. 1–11, 2023.
- [334] D. Z. Chen et al. Text2tex: Text-driven texture synthesis via diffusion models. In *ICCV*, pp. 18558–18568, 2023.
- [335] D. Z. Chen et al. Scenetex: High-quality texture synthesis for indoor scenes via diffusion priors. *arXiv preprint arXiv:2311.17261*, 2023.
- [336] R. Jiang et al. Avatarcraft: Transforming text into neural human avatars with parameterized shape and pose control. In *ICCV*, pp. 14371–14382, 2023.
- [337] F. Hong et al. Avatarclip: Zero-shot text-driven generation and animation of 3d avatars. *ACM TOG*, 41(4):1–19, 2022.
- [338] C. Diller and A. Dai. Cg-hoi: Contact-guided 3d human-object interaction generation. In *CVPR*, 2024.
- [339] L. Li and A. Dai. Genzi: Zero-shot 3d human-scene interaction generation. In *CVPR*, 2024.
- [340] A. Vilesov et al. Cg3d: Compositional generation for text-to-3d via gaussian splatting. *arXiv preprint arXiv:2311.17907*, 2023.
- [341] R. Po and G. Wetzstein. Compositional 3d scene generation using locally conditioned diffusion. *arXiv preprint arXiv:2303.12218*, 2023.
- [342] G. Gao et al. Graphdreamer: Compositional 3d scene synthesis from scene graphs. In *CVPR*, 2024.
- [343] Z. Ziyu et al. 3d-vista: Pre-trained transformer for 3d vision and text alignment. In *ICCV*, 2023.
- [344] B. Chen et al. Spatialvlm: Endowing vision-language models with spatial reasoning capabilities. *arXiv preprint arXiv:2401.12168*, 2024.
- [345] A. Delitzas et al. Multi-clip: Contrastive vision-language pre-training for question answering tasks in 3d scenes. *arXiv preprint arXiv:2306.02329*, 2023.
- [346] Z. Yuan et al. Instancerefer: Cooperative holistic understanding for visual grounding on point clouds through instance multi-level contextual referring. In *ICCV*, pp. 1791–1800, 2021.
- [347] J. Roh et al. Languagerefer: Spatial-language model for 3d visual grounding. In *Conference on Robot Learning*, pp. 1046–1056. PMLR, 2022.
- [348] L. Zhao et al. 3dvg-transformer: Relation modeling for visual grounding on point clouds. In *ICCV*, pp. 2928–2937, 2021.
- [349] T. Luo et al. Scalable 3d captioning with pretrained models. *NeurIPS*, 36, 2024.
- [350] K. Chen et al. Text2shape: Generating shapes from natural language by learning joint embeddings. In *ACCV*, pp. 100–116. Springer, 2019.
- [351] B. Jia et al. Sceneverse: Scaling 3d vision-language learning for grounded scene understanding. *arXiv preprint arXiv:2401.09340*, 2024.
- [352] T. Wang et al. Embodiedscan: A holistic multi-modal 3d perception suite towards embodied ai. *arXiv preprint arXiv:2312.16170*, 2023.
- [353] A. Abdelreheem et al. Scanents3d: Exploiting phrase-to-3d-object correspondences

- for improved visio-linguistic models in 3d scenes. In *WACV*, pp. 3524–3534, 2024.
- [354] Z. Lin et al. Wildrefer: 3d object localization in large-scale dynamic scenes with multi-modal visual data and natural language. *arXiv preprint arXiv:2304.05645*, 2023.
- [355] T. Miyanishi et al. Cross3dvg: Baseline and dataset for cross-dataset 3d visual grounding on different rgb-d scans. *arXiv preprint arXiv:2305.13876*, 2023.
- [356] S. Kato et al. Arkitscenerefer: Text-based localization of small objects in diverse real-world 3d indoor scenes. In *Findings of the Association for Computational Linguistics: EMNLP 2023*, pp. 784–799, 2023.
- [357] S. Ye et al. 3d question answering, 2021.
- [358] X. Yan et al. Comprehensive visual question answering on point clouds through compositional scene manipulation. *IEEE Transactions on Visualization & Computer Graphics*, pp. 1–13, 2023.
- [359] M. Li et al. M3dbench: Let’s instruct large models with multi-modal 3d prompts. *arXiv preprint arXiv:2312.10763*, 2023.
- [360] Z. Yin et al. Lamm: Language-assisted multi-modal instruction-tuning dataset, framework, and benchmark. *arXiv preprint arXiv:2306.06687*, 2023.
- [361] A. Dai et al. Scannet: Richly-annotated 3d reconstructions of indoor scenes. In *CVPR*, 2017.
- [362] F. Zeng et al. Large language models for robotics: A survey. *arXiv preprint arXiv:2311.07226*, 2023.
- [363] H. Zhou et al. Language-conditioned learning for robotic manipulation: A survey. *arXiv preprint arXiv:2312.10807*, 2023.
- [364] H. Caesar et al. nuscenes: A multimodal dataset for autonomous driving. *arXiv preprint arXiv:1903.11027*, 2019.
- [365] OpenAI. Gpt-4 technical report. *arXiv preprint arXiv:2303.08774*, 2023.
- [366] A. Kirillov et al. Segment anything. *arXiv preprint arXiv:2304.02643*, 2023.
- [367] P. Cong et al. Stcrowd: A multimodal dataset for pedestrian perception in crowded scenes. In *CVPR*, pp. 19608–19617, 2022.
- [368] G. Baruch et al. Arkitscenes: A diverse real-world dataset for 3d indoor scene understanding using mobile rgb-d data. *arXiv preprint arXiv:2111.08897*, 2021.
- [369] S. K. Ramakrishnan et al. Habitat-matterport 3d dataset (HM3d): 1000 large-scale 3d environments for embodied AI. In *Thirty-fifth Conference on Neural Information Processing Systems Datasets and Benchmarks Track (Round 2)*, 2021.
- [370] K. Yadav et al. Habitat-matterport 3d semantics dataset. *arXiv preprint arXiv:2210.05633*, 2022.
- [371] J. Wald et al. Learning 3d semantic scene graphs from 3d indoor reconstructions. In *CVPR*, 2020.